EFFECT OF ENVIRONMENTAL TORQUES ON SHORT-TERM ATTITUDE PREDICTION FOR A ROLLING-WHEEL SPACECRAFT IN A SUN-SYNCHRONOUS ORBIT

by Ward F. Hodge

Langley Research Center
Hampton, Va. 23365

NATIONAL AERONAUTICS AND SPACE ADMINISTRATION • WASHINGTON, D. C. • JANUARY 1972

1. Report No.	2. Government Accession No.	3. Recipient's Catalog No.
NASA TN D-6583		

4. Title and Subtitle	5. Report Date
EFFECT OF ENVIRONMENTAL TORQUES ON SHORT-TERM ATTITUDE PREDICTION FOR A ROLLING-WHEEL SPACECRAFT IN A SUN-SYNCHRONOUS ORBIT	January 1972
	6. Performing Organization Code
7. Author(s)	8. Performing Organization Report No.
Ward F. Hodge	L-7359
	10. Work Unit No.
9. Performing Organization Name and Address	115-17-07-01
NASA Langley Research Center Hampton, Va. 23365	11. Contract or Grant No.
	13. Type of Report and Period Covered
12. Sponsoring Agency Name and Address	Technical Note
National Aeronautics and Space Administration Washington, D.C. 20546	14. Sponsoring Agency Code

15. Supplementary Notes

16. Abstract

A numerical evaluation and an analysis of the effects of environmental disturbance torques on the attitude of a hexagonal cylinder rolling-wheel spacecraft were performed. The resulting perturbations caused by five such torques were found to be very small and exhibited linearity such that linearized equations of motion yielded accurate results over short periods and the separate perturbations contributed by each torque were additive in the sense of superposition. Linearity of the torque perturbations was not affected by moderate system design changes and persisted for torque-to-angular momentum ratios up to 100 times the nominal expected value. As these conditions include many possible applications, similar linear behavior might be anticipated for other rolling-wheel spacecraft.

17. Key Words (Suggested by Author(s))	18. Distribution Statement
Attitude prediction Rigid-body motions Environmental torques	Unclassified – Unlimited

19. Security Classif. (of this report)	20. Security Classif. (of this page)	21. No. of Pages	22. Price*
Unclassified	Unclassified	52	$3.00

*For sale by the National Technical Information Service, Springfield, Virginia 22151

EFFECT OF ENVIRONMENTAL TORQUES ON SHORT-TERM ATTITUDE PREDICTION FOR A ROLLING-WHEEL SPACECRAFT IN A SUN-SYNCHRONOUS ORBIT

By Ward F. Hodge
Langley Research Center

SUMMARY

The change in attitude produced by the action of environmental disturbance torques was investigated for a hexagonal cylinder spacecraft in a nearly polar 500-kilometer circular orbit. A numerical evaluation and an analysis of the separate and combined effects of five such torques, arising from gravitational, magnetic, and surface pressure forces, were performed. The resulting perturbations were determined from time histories of the basic attitude state variables generated by numerical integration of the spacecraft equations of motion covering about one-third of the orbital period. Similar data were generated for examining linearity of the torque perturbations and sensitivities to system design changes and torque coefficient variations.

The torque perturbations proved to be very small and exhibited linearity such that linearized equations of motion yielded accurate results over short periods and the separate perturbations contributed by the individual torques were additive in the sense of superposition. Linearity of the torque perturbations was not affected by moderate system design changes and persisted for torque-to-angular momentum ratios up to 100 times the expected 10^{-7} nominal value. As these conditions include many possible applications, similar linear behavior might be anticipated for other rolling-wheel spacecraft.

The principal perturbations consisted of a relatively small spin decay of about 1^{o} caused primarily by eddy-current torque, and a slight spin-axis drift of some 70 arc-seconds due mainly to solar radiation pressure and magnetic-moment torques. Because of the small 10^{-7} torque-to-angular momentum ratio, the affected torque terms in the spacecraft equations of motion remain so small that Euler-angle singularities are unlikely to be approached closely enough to cause difficulties. In regard to attitude prediction, the environmental torques were estimated to have a much lesser effect than the propagation of state estimation residuals.

INTRODUCTION

The use of spin-stabilized satellites for conducting measurements research, in fields such as earth resources and meteorology, generally requires precise spacecraft attitude information over extended periods. For such applications, the line of sight of an instrument axis fixed in the spacecraft must be known within about 15 arc-seconds during data-gathering periods to obtain results having the desired spatial resolution. This problem was investigated as part of recent studies of spacecraft configurations and instrumentation for high resolution measurements of the earth's infrared horizon profile conducted or sponsored by the NASA Langley Research Center.

The stringent accuracy required for this type of mission necessitates frequent updating of the spacecraft attitude to prevent the propagation of state estimation residuals and dynamical modeling uncertainties from causing the allowable pointing error to be exceeded. Attitude prediction or state transition over long periods is therefore not feasible, and a short-term approach must be implemented. The scheme employed for the horizon measurements studies assumes the necessary updating can be satisfactorily accomplished by means of precise attitude estimation. Based on operational limitations which affect the availability of attitude determination data, the maximum interval between updates for which attitude prediction would be required is about one-third of the spacecraft orbital period.

In seeking a suitable analytical procedure for achieving the required attitude accuracy and handling problems such as Euler-angle singularities, two alternate choices for the basic attitude state variables were studied independently and concurrently. Because of their influence on attitude prediction, an important task in each case was to model and evaluate with care the effects of significant disturbance torques. The systems study of reference 1 and the excerpt from it given in reference 2 contain torque calculations based on the use of state variables comprised of the body-axis components of the spacecraft angular velocity, and aircraft-type Euler angles analogous to yaw, pitch, and roll. While the computations from both studies were essentially in agreement, a more extensive evaluation of the torques and their effects was performed by using the angular momentum formulation described in the present paper. The results and conclusions obtained are more general than those of references 1 and 2, and the analysis presented includes linearity of the torque perturbations, sensitivities to system design changes, and Euler-angle singularities. In summarizing the overall investigation, the two approaches were compared and the use of time-averaged equations of motion such as those of reference 3 were discussed.

SYMBOLS

A	area of spacecraft panel exposed to surface pressure, centimeters^2
A_x, A_y, A_z	aerodynamic pressure torque coefficients, dyne-centimeters
a	altitude, kilometers
B	geomagnetic field intensity or flux density, teslas
b	height of spacecraft side panels, centimeters
$C(\lambda_o, \Phi_o, \zeta_o)$	spacecraft panel orientation matrix (eq. (B3))
c	spacecraft eddy-current coefficient, meters^4/ohm
$E(\phi, \theta, \psi)$	spacecraft Euler-angle matrix (eq. (3))
e	eccentricity of spacecraft orbit
$e_{j,k}$	elements of $E(\phi, \theta, \psi)$
F	surface pressure force, dynes
$G(\alpha, \Theta)$	geomagnetic field matrix (eq. (A5))
g_n^m, h_n^m	Schmidt-normalized Gaussian coefficients, nanoteslas
$H(\xi, \tau)$	spacecraft angular momentum vector orientation matrix (eq. (2))
h	spacecraft angular momentum, dyne-centimeter-seconds
I_x, I_y, I_z	spacecraft principal moments of inertia, gram-centimeters^2
i	inclination of spacecraft orbit, degrees
L	geocentric true longitude of sun on ecliptic, degrees
l	length of spacecraft solar cell panels, centimeters

M	spacecraft residual magnetic moment, ampere(turn)-meters^2
n_o	spacecraft mean orbital motion, radians/second
$P_n^m(\Theta)$	Schmidt-normalized associated Legendre function
$\hat{p}$	unit vector along incident direction of a surface pressure
q_o	aerodynamic pressure, dynes/centimeter^2
R_x, R_y, R_z	solar radiation pressure torque coefficients, dyne-centimeters
r	radius, centimeters
r_a	mean radius of earth, kilometers
r_o	geocentric distance of spacecraft, kilometers
$r_\oplus$	equatorial radius of earth, kilometers
S	intensity of solar radiation pressure, dynes/centimeter^2
s	fraction of ρ reflected specularly (eqs. (B8))
T	environmental torque, dyne-centimeters
t	time, seconds
u	argument of latitude of spacecraft orbit, degrees
v_o	linear velocity along spacecraft orbital path, kilometers/second
$W(\Omega,i,u)$	orbit orientation matrix (eq. (1))
w	width of spacecraft panels, centimeters
x,y,z	rectangular coordinates and spacecraft principal axes
α	geocentric right ascension, degrees

α_o	effective spacecraft angle of attack, degrees
β	solar elevation phase angle, degrees
$\gamma_x,\gamma_y,\gamma_z$	direction cosines of $\vec{r}_o$ relative to spacecraft principal axes
δ	geocentric declination, degrees
ϵ	obliquity of ecliptic, degrees
η	surface pressure angle of incidence, degrees
Θ	geocentric colatitude, degrees
λ	geocentric longitude, measured east from Greenwich meridian, degrees
λ_o,Φ_o,ζ_o	spacecraft panel orientation angles, degrees
μ	universal gravitational constant, kilometers^3/second^2
ν	surface pressure azimuth relative to a spacecraft panel, degrees
ξ	geocentric right ascension of $\vec{h}$, degrees
ρ	fraction of incident solar radiation reflected by A (eqs. (B8))
ρ_o	atmospheric density, kilograms/meter^3
σ_N,σ_T	aerodynamic pressure surface reflection coefficients for normal and tangential momentum exchange
τ	geocentric codeclination of $\vec{h}$, degrees
Φ	sum of Euler angles ϕ and ψ, degrees
ϕ,θ,ψ	spacecraft Euler angles, degrees
Ω	geocentric right ascension of ascending node of spacecraft orbit, degrees

ω	spacecraft angular velocity, radians/second
$\omega_{\oplus}$	axial rotation rate of earth, radians/second

Subscripts:

G	Greenwich meridian
h	angular momentum
i	inertial
j,k	matrix element indices
N	normal component
n	degree of spherical harmonic expansion
o	orbital, initial, or reference value
T	tangential component
x,y,z	spacecraft principal axis components
Θ,λ,r	geocentric spherical polar components

Superscript:

m	order of spherical harmonic expansion

Notation:

'	transformed, deviated, or compared quantity
$\cdot$	time derivative
$\hat{}$	unit vector
$\rightarrow$	vector

–	centroidal distance
≐	centroidal vector
-1	matrix inverse
Δ	residual or differential value
$\widehat{\text{sec}}$	arc-second

ANALYTICAL FORMULATION

The angular momentum formulation used in the study is described in two steps which respectively define the spacecraft system and the dynamics of the rigid-body motion. The first concerns the spacecraft configuration, orbit, and attitude, and the second, the equations of motion and modeling of the environmental disturbance torques.

Spacecraft Configuration

The basic spacecraft assumed for both studies was a rolling-wheel vehicle in the form of a right hexagonal cylinder having six solar cell panels attached to one base. As depicted in figure 1, this configuration consisted of two hexagonal end panels of width 2w across corners, six side panels of width w and height b, and six solar cell panels of negligible thickness, width w, and length l. The spacecraft principal axes x, y, and z and center of mass were assumed to have the orientations indicated in the sketch. The dimensions w, b, and l and other pertinent spacecraft data are listed in table I.

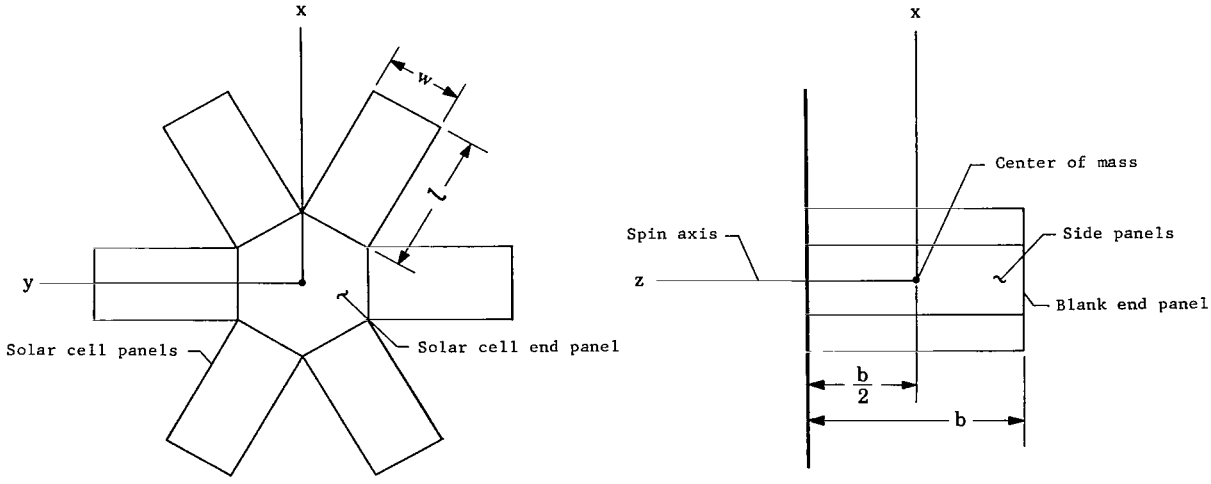

Figure 1.- Hexagonal spacecraft configuration.

Spacecraft Orbit

A geocentric equatorial coordinate system x_i,y_i,z_i, having x_i toward the vernal equinox and z_i along the earth's spin axis as shown in figure 2, was used as the inertial

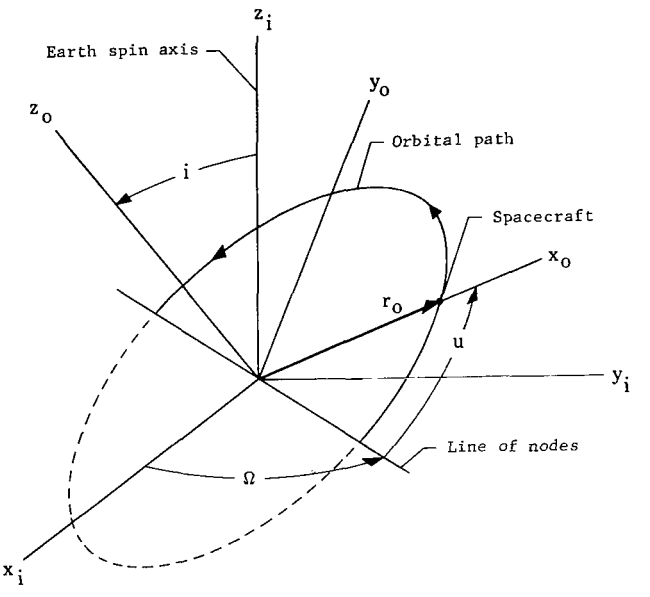

Figure 2.- Spacecraft orbit.

reference for both the spacecraft orbital and rigid-body motions. The orientation of the spacecraft orbit relative to these axes is defined by the three angles Ω, i, and u as indicated. Let x_o, y_o, and z_o be a set of rotating axes alined with the orbit plane such that z_o coincides with the normal to the orbit plane and x_o is along the local vertical. The transformation between the orbital and inertial coordinate systems is then

$$\begin{pmatrix} x_o \\ y_o \\ z_o \end{pmatrix} = W(\Omega,i,u) \begin{pmatrix} x_i \\ y_i \\ z_i \end{pmatrix} \tag{1}$$

where

$$W(\Omega,i,u) = \begin{pmatrix} \cos u \cos \Omega - \cos i \sin u \sin \Omega & \cos u \sin \Omega + \cos i \sin u \cos \Omega & \sin u \sin i \\ -\sin u \cos \Omega - \cos i \cos u \sin \Omega & -\sin u \sin \Omega + \cos i \cos u \cos \Omega & \cos u \sin i \\ \sin i \sin \Omega & -\sin i \cos \Omega & \cos i \end{pmatrix}$$

The relevant physical data and values assumed for the orbital elements may be found in tables II and III, respectively.

Spacecraft Attitude and Pointing Direction

The manner in which the angular momentum state variables define the spacecraft attitude is described. Then the angular coordinates of a spacecraft axis, chosen to represent the line-of-sight or pointing-direction reference for onboard instrumentation, are expressed as functions of these variables.

State variables.- The angular momentum state variables express the spacecraft attitude in terms of five angles and the magnitude of the angular momentum vector. The first two angles ξ and τ define the inertial direction of the angular momentum vector $\vec{h}$, and the remaining three angles ϕ, θ, and ψ give the orientation of the spacecraft principal axes x, y, and z relative to $\vec{h}$. Figure 3 illustrates the definitions of

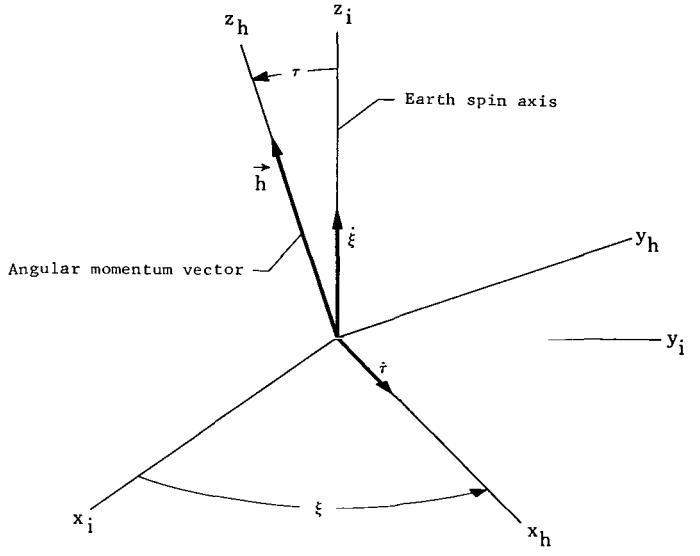

Figure 3.- Orientation of spacecraft angular momentum vector.

ξ and τ, and an angular momentum coordinate system x_h, y_h, z_h chosen such that z_h coincides with $\vec{h}$. The transformation of these axes to inertial reference is

$$\begin{pmatrix} x_h \\ y_h \\ z_h \end{pmatrix} = H(\xi,\tau) \begin{pmatrix} x_i \\ y_i \\ z_i \end{pmatrix} \tag{2}$$

where

$$H(\xi,\tau) = \begin{pmatrix} \cos\xi & \sin\xi & 0 \\ -\sin\xi\cos\tau & \cos\xi\cos\tau & \sin\tau \\ \sin\xi\sin\tau & -\cos\xi\sin\tau & \cos\tau \end{pmatrix}$$

The Euler angles ϕ, θ, and ψ, which relate the principal axes to the system x_h, y_h, z_h in the manner shown in figure 4, complete the definition of the spacecraft

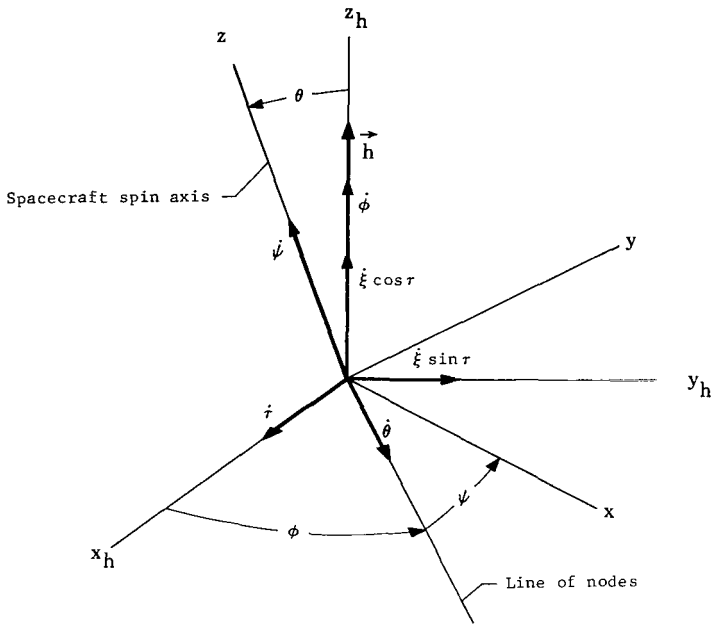

Figure 4.- Spacecraft principal axes and Euler angles.

attitude in terms of the angular momentum state variables. The x-, y-, and z-axes and x_h-, y_h-, and z_h-axes are related by

$$\begin{pmatrix} x \\ y \\ z \end{pmatrix} = E(\phi,\theta,\psi) \begin{pmatrix} x_h \\ y_h \\ z_h \end{pmatrix} \tag{3}$$

where

$$E(\phi,\theta,\psi) = \begin{pmatrix} \cos\psi\cos\phi - \cos\theta\sin\phi\sin\psi & \cos\psi\sin\phi + \cos\theta\cos\phi\sin\psi & \sin\psi\sin\theta \\ -\sin\psi\cos\phi - \cos\theta\sin\phi\cos\psi & -\sin\psi\sin\phi + \cos\theta\cos\phi\cos\psi & \cos\psi\sin\theta \\ \sin\theta\sin\phi & -\sin\theta\cos\phi & \cos\theta \end{pmatrix}$$

Pointing direction.- The geocentric right ascension α and declination δ of the principal axis x were used to define the spacecraft pointing direction as indicated in figure 5. As the instrument line of sight was intended to be perpendicular to the spin axis z, this choice provides a suitable basis for determining the net change in pointing direction caused by the torques. Expressions for evaluating α and δ in terms of the state variables ξ, τ, ϕ, θ, and ψ were obtained by equating the direction cosines of

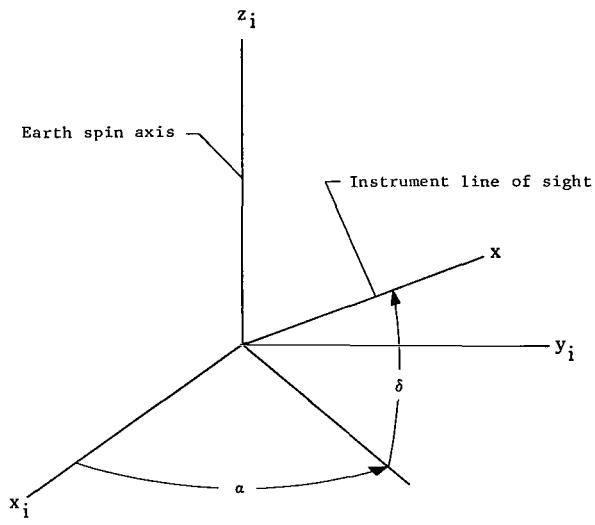

Figure 5.- Spacecraft pointing direction.

the x-axis as defined by α and δ in figure 5 with those resulting from the total transformation given by equations (2) and (3). The desired relationship is

$$\begin{pmatrix} \cos\delta\cos\alpha \\ \cos\delta\sin\alpha \\ \sin\delta \end{pmatrix} = \begin{pmatrix} e_{11}\cos\xi - \sin\xi(e_{12}\cos\tau - e_{13}\sin\tau) \\ e_{11}\sin\xi + \cos\xi(e_{12}\cos\tau - e_{13}\sin\tau) \\ e_{12}\sin\tau + e_{13}\cos\tau \end{pmatrix}$$

from which

$$\left.\begin{aligned} \tan\alpha &= \frac{e_{11}\sin\xi + \cos\xi\,(e_{12}\cos\tau - e_{13}\sin\tau)}{e_{11}\cos\xi - \sin\xi\,(e_{12}\cos\tau - e_{13}\sin\tau)} \\ \sin\delta &= e_{12}\sin\tau + e_{13}\cos\tau \end{aligned}\right\} \qquad (4)$$

where e_{11}, e_{12}, and e_{13} and the right-hand members of equations (4) are the elements of the first rows of $\mathbf{E}$ and the product $\mathbf{EH}$, respectively.

Equations of Motion

Although the customary form of Euler's dynamical equations provides a suitable description of the spacecraft rigid-body motion, equivalent first-order expressions for the rates of the six state variables were used instead. These equations are somewhat

more convenient for numerical integration and differ only slightly from those of reference 4 which extend earlier formulations (for example, see ref. 5) to include torques. The expressions for $\dot{\xi}$, $\dot{\tau}$, $\dot{h}$, $\dot{\phi}$, $\dot{\theta}$, and $\dot{\psi}$ used in the study were obtained as follows. By starting with the equation for the torque about the center of mass of a rigid body

$$\left.\begin{aligned} &\vec{T} = \dot{\vec{h}} + \left(\vec{\omega} \times \vec{h}\right) \\ &\text{or} \\ &\begin{pmatrix} T_x \\ T_y \\ T_z \end{pmatrix} = \begin{pmatrix} \dot{h}_x \\ \dot{h}_y \\ \dot{h}_z \end{pmatrix} + \begin{pmatrix} \omega_y h_z - \omega_z h_y \\ -\omega_x h_z + \omega_z h_x \\ \omega_x h_y - \omega_y h_x \end{pmatrix} \end{aligned}\right\} \tag{5}$$

the principal axis components of $\vec{h}$

$$\left.\begin{aligned} h_x &= I_x \omega_x = h \sin\theta \sin\psi \\ h_y &= I_y \omega_y = h \sin\theta \cos\psi \\ h_z &= I_z \omega_z = h \cos\theta \end{aligned}\right\} \tag{6}$$

may be used to eliminate the components of $\vec{\omega}$ from equations (5). Substitution of equations (6) and their time derivatives into equations (5) gives

$$T_x = \dot{h} \sin\theta \sin\psi + h\left(\dot{\theta} \cos\theta \sin\psi + \dot{\psi} \sin\theta \cos\psi\right) + h^2 \sin\theta \cos\theta \cos\psi \left(\frac{1}{I_y} - \frac{1}{I_z}\right)$$

$$T_y = \dot{h} \sin\theta \cos\psi + h\left(\dot{\theta} \cos\theta \cos\psi - \dot{\psi} \sin\theta \sin\psi\right) - h^2 \sin\theta \cos\theta \sin\psi \left(\frac{1}{I_x} - \frac{1}{I_z}\right)$$

$$T_z = \dot{h} \cos\theta - h\,\dot{\theta} \sin\theta + h^2 \sin^2\theta \sin\psi \cos\psi \left(\frac{1}{I_x} - \frac{1}{I_y}\right)$$

from which

$$\dot{h} = \left(T_x \sin\psi + T_y \cos\psi\right) \sin\theta + T_z \cos\theta$$

$$\dot{\theta} = h \sin\theta \sin\psi \cos\psi \left(\frac{1}{I_x} - \frac{1}{I_y}\right) + \frac{1}{h}\left[\left(T_x \sin\psi + T_y \cos\psi\right) \cos\theta - T_z \sin\theta\right]$$

$$\dot{\psi} = h \cos\theta \left(\frac{1}{I_z} - \frac{\sin^2\psi}{I_x} - \frac{\cos^2\psi}{I_y}\right) + \frac{1}{h \sin\theta}\left(T_x \cos\psi - T_y \sin\psi\right)$$

The remaining three equations were obtained in a similar manner by substituting another definition of the components of $\vec{\omega}$ into equations (5). Reference to figure 4 shows that

$$\begin{pmatrix} \omega_x \\ \omega_y \\ \omega_z \end{pmatrix} = E(\phi,\theta,\psi) \begin{pmatrix} \dot{\tau} \\ \dot{\xi} \sin \tau \\ \dot{\xi} \cos \tau \end{pmatrix} + \begin{pmatrix} \dot{\phi} \sin \theta \sin \psi + \dot{\theta} \cos \psi \\ \dot{\phi} \sin \theta \cos \psi - \dot{\theta} \sin \psi \\ \dot{\phi} \cos \theta + \dot{\psi} \end{pmatrix} \tag{7}$$

where the first term on the right-hand side accounts for the angular velocity of $\vec{h}$. By substituting equations (7) into equations (5) and performing the indicated algebraic reductions

$$T_x = \dot{h} \sin \theta \sin \psi + h\left(-e_{12}\dot{\tau} + e_{11}\dot{\xi} \sin \tau\right)$$

$$T_y = \dot{h} \sin \theta \cos \psi - h\left(e_{22}\dot{\tau} - e_{21}\dot{\xi} \sin \tau\right)$$

$$T_z = \dot{h} \cos \theta + h \sin \theta \left(\dot{\tau} \cos \phi + \dot{\xi} \sin \tau \sin \phi\right)$$

which may be solved for

$$\dot{\tau} = -\frac{1}{h \sin \theta}\left[\dot{h} \cos \theta \cos \phi + \sin \theta \sin \phi \left(T_x \cos \psi - T_y \sin \psi\right) - T_z \cos \phi\right]$$

and

$$\dot{\xi} = \frac{1}{h \sin \tau \sin \theta}\left[-\dot{h} \cos \theta \sin \phi + \sin \theta \cos \phi \left(T_x \cos \psi - T_y \sin \psi\right) + T_z \sin \phi\right]$$

where $\dot{h}$ is given by the expression previously obtained. Substituting ω_z from equations (7) into the third member of equations (6) and solving for $\dot{\phi}$ gives

$$\dot{\phi} = \frac{h}{I_z} - \frac{\dot{\psi}}{\cos \theta} - \dot{\xi} \cos \tau - \tan \theta \left(\dot{\tau} \sin \phi - \dot{\xi} \sin \tau \cos \phi\right)$$

Thus the complete set of equations is

$$
\left.
\begin{aligned}
\dot{h} &= \left(T_x \sin\psi + T_y \cos\psi\right)\sin\theta + T_z \cos\theta \\
\dot{\xi} &= \frac{1}{h \sin\tau}\left[\cos\phi\left(T_x \cos\psi - T_y \sin\psi\right) - \cos\theta \sin\phi\left(T_x \sin\psi + T_y \cos\psi\right) + T_z \sin\theta \sin\phi\right] \\
\dot{\tau} &= -\frac{1}{h}\left[\sin\phi\left(T_x \cos\psi - T_y \sin\psi\right) + \cos\theta \cos\phi\left(T_x \sin\psi + T_y \cos\psi\right) - T_z \sin\theta \cos\phi\right] \\
\dot{\phi} &= h\left(\frac{\sin^2\psi}{I_x} + \frac{\cos^2\psi}{I_y}\right) - \frac{\cot\theta}{h}\left(T_x \cos\psi - T_y \sin\psi\right) - \dot{\xi}\cos\tau \\
\dot{\theta} &= h \sin\theta \sin\psi \cos\psi\left(\frac{1}{I_x} - \frac{1}{I_y}\right) + \frac{1}{h}\left[\left(T_x \sin\psi + T_y \cos\psi\right)\cos\theta - T_z \sin\theta\right] \\
\dot{\psi} &= h \cos\theta\left(\frac{1}{I_z} - \frac{\sin^2\psi}{I_x} - \frac{\cos^2\psi}{I_y}\right) + \frac{1}{h \sin\theta}\left(T_x \cos\psi - T_y \sin\psi\right)
\end{aligned}
\right\} \quad (8)
$$

Environmental Torques

Of the possible sources of disturbance torques, only those arising from gravitational, magnetic, and surface pressure forces appeared large enough to affect the spacecraft attitude. The resulting analytical model consisted of five environmental torques due to gravity gradient, magnetic moment, eddy current, solar radiation pressure, and aerodynamic pressure. All other torques were estimated to be either negligible over the short intervals being considered or rendered insignificant by a systems operation constraint that all energy radiators, dampers, and control systems be deactivated during data-gathering periods for which precise attitude information is required. Torque sources such as mass expulsion and momentum transfer were further minimized by using magnetic coils in place of gas-operated and momentum exchange control devices.

For the spacecraft inertia configuration assumed in table I, the spherical earth gravity-gradient torque model given in reference 6 was considered adequate. The torques due to interaction with the geomagnetic field were evaluated from the well-known equations appearing in reference 7 and the field computation procedure described in appendix A. As the torques arising from surface pressure forces are highly dependent on the geometry and orientation of the spacecraft surfaces, the solar radiation and aerodynamic pressure torque equations usually must be formulated to suit the application. The equations developed in appendix B for the hexagonal configuration are based on the surface pressure force models contained in references 8 and 9.

Gravity gradient.- According to the spherical earth model, the principal axis components of the gravity-gradient torque are

$$\left.\begin{aligned} T_x &= 3n_o^2(I_z - I_y)\gamma_y\gamma_z \\ T_y &= 3n_o^2(I_x - I_z)\gamma_x\gamma_z \\ T_z &= 3n_o^2(I_y - I_x)\gamma_x\gamma_y \end{aligned}\right\} \tag{9}$$

where $n_o = \sqrt{\mu/r_o^3}$ is the spacecraft mean orbital motion (see table III) and

$$\begin{pmatrix} \gamma_x \\ \gamma_y \\ \gamma_z \end{pmatrix} = EHW^{-1}\begin{pmatrix} -1 \\ 0 \\ 0 \end{pmatrix} \tag{10}$$

are the direction cosines of the gravitational attraction force with respect to the x, y, and z principal axes as obtained from equations (1) to (3).

Magnetic moment.- The torque caused by the interaction of the residual magnetic moment of the spacecraft with the geomagnetic field is

$$\left.\begin{aligned} &\vec{T} = \vec{M} \times \vec{B} \\ &\text{or} \\ T_x &= M_yB_z - M_zB_y \\ T_y &= M_zB_x - M_xB_z \\ T_z &= M_xB_y - M_yB_x \end{aligned}\right\} \tag{11}$$

where the values assumed for M_x, M_y, and M_z are listed in table I, and B_x, B_y, and B_z may be evaluated by means of the procedure described in appendix A.

Eddy current.- Assuming the spacecraft hull to be approximated as a thin spherical shell, the torque due to eddy-current circulation is

$$\vec{T} = c\left(\vec{\omega} \times \vec{B}\right) \times \vec{B}$$

or

$$\left.\begin{aligned} T_X &= -c\left[\omega_X\left(B_y^2 + B_z^2\right) - B_X\left(B_y\omega_y + B_z\omega_z\right)\right] \\ T_y &= -c\left[\omega_y\left(B_x^2 + B_z^2\right) - B_y\left(B_x\omega_x + B_z\omega_z\right)\right] \\ T_Z &= -c\left[\omega_z\left(B_x^2 + B_y^2\right) - B_z\left(B_x\omega_x + B_y\omega_y\right)\right] \end{aligned}\right\} \tag{12}$$

where the value used for the eddy-current coefficient c is also listed in table I and ω_X, ω_y, and ω_Z may be computed from either equations (6) or (7). The adequacy of equations (12) for the hexagonal configuration was demonstrated in references 1 and 2 where a more elaborate cylindrical shell model was shown to be unnecessary.

Solar radiation pressure.- Based on the evaluation performed in appendix B, the principal axis components of the solar radiation pressure torque were assumed to be reasonably approximated as

$$\left.\begin{aligned} T_X &= -R_X \sin(\Phi - \beta) \\ T_y &= -R_y \cos(\Phi - \beta) \\ T_Z &= R_Z \sin 6(\Phi - \beta) \end{aligned}\right\} \tag{13}$$

where $\Phi = \phi + \psi$ and β is a solar elevation phase angle (see appendix B). The values derived for the torque coefficients R_X, R_y, and R_Z may be found in table I.

Aerodynamic pressure.- A similar evaluation (see appendix B) yielded

$$\left.\begin{aligned} T_X &= A_X\left|\sin\alpha_o\right| \cos u \cos(\Phi - u) \\ T_y &= -A_y\left|\sin\alpha_o\right| \cos u \sin(\Phi - u) \\ T_Z &= -A_Z \sin\alpha_o \cos u \sin 6(\Phi - u) \end{aligned}\right\} \tag{14}$$

for the principal axis components of the aerodynamic pressure torque where α_o is the effective angle of attack and A_X, A_y, and A_Z are also derived torque coefficients (see table I).

RESULTS AND ANALYSIS

A numerical evaluation and an analysis of the torqued spacecraft motion, based on equations (8) to (14), were performed for the nominal conditions and data listed in tables I to III. The procedures employed for numerically integrating these equations and determining the total instrument-axis pointing error are described; then the deviations or perturbations caused by the environmental torques are analyzed. These quantities were calculated from time histories of the state variables covering 2000 seconds or about a third of the orbital period, which was the maximum prediction interval required as stated in the introduction. Typical results for only one 2000-second period are presented since time histories obtained for nominal and worst case conditions indicated that the nature of the torque perturbations should remain essentially the same for all such intervals. Lastly, the angular velocity and angular momentum formulations were compared, and the use of time-averaged equations of motion was discussed.

Approach

The computational considerations addressed in generating the necessary time histories were the choice of numerical method, comparison of direct and perturbation solutions of equations (8), effect of singularities on the use of angular momentum state variables, and calculation of the instrument-axis pointing error.

Numerical integration.- As equations (8) are of first order and the torques are very small, the fourth-order Runge-Kutta scheme was chosen as the integration method. The integration step was determined by progressively reducing the step size until successive solutions differed by less than the equivalent of 2 arc-seconds in all six state variables over the full 2000-second integration period. This level was reached when the step size was decreased from 0.1 to 0.01 second. A step size of 0.1 second thus appeared adequate and was chosen in anticipation that the total integration error due to truncation and round-off probably would not exceed a few arc-seconds.

In order to determine whether a perturbation approach would be advantageous, time histories generated from equations linearized about the untorqued solution of equations (8) were compared with corresponding ones obtained by direct integration. Both methods were found to give essentially the same results over the entire 2000-second period with no rectification of the linearized solution, thus indicating that the small torque perturbations were accurately approximated by using the linearized equations.

Euler-angle singularities.- Inspection of equations (8) shows that singularities will occur if either θ or τ is zero. The latter was of no concern as attitude control will constrain τ to within 5° of the nominal 97.72° value listed in table III, but the θ-singularity could occur since the spacecraft was intended to spin without coning. However, no difficulty was encountered for the 0.66° coning angle assumed for the study.

This result was verified by repeating the computations using the angular velocity state variables of references 1 and 2 which avoid all singularities for the conditions being considered. The two sets of values for the instrument-axis coordinates α and δ were identical within a few hundredths of an arc-second.

The reason small values of θ caused no trouble stems from the smallness of the ratio of $T_x \cos \psi - T_y \sin \psi$ to h in the fourth and sixth members of equations (8). Comparison of this ratio, which was the order of 10^{-7} for the data given in tables I and III, with $\sin \theta$ shows that θ could approach zero within a few arc-seconds before the affected torque terms become even as large as the untorqued ones. The likelihood of θ becoming this small appears remote because the minimum initial coning angle achievable with existing nutation dampers is limited by factors such as tuning errors and residual spacecraft imbalance. Further inspection of equations (8) indicates that τ also could be within a few arc-seconds of zero without causing difficulty for the same reason. Thus, the use of angular momentum state variables for the horizon measurement spacecraft does not appear to be restricted by either singularity and need not be avoided.

Instrument-axis pointing error.- The uncertainty in the instrument line of sight, which ultimately must be determined, was considered to be suitably represented by the total change in the pointing direction of the assumed instrument axis. This quantity gives a direct measure of the total line-of-sight error caused by the torques and clearly indicates the relative significance of each torque. The pointing-direction error was defined to be the total change in the inertial orientation of the assumed instrument axis (see fig. 5). This angle is denoted as Δx in figure 6 and may be readily calculated from

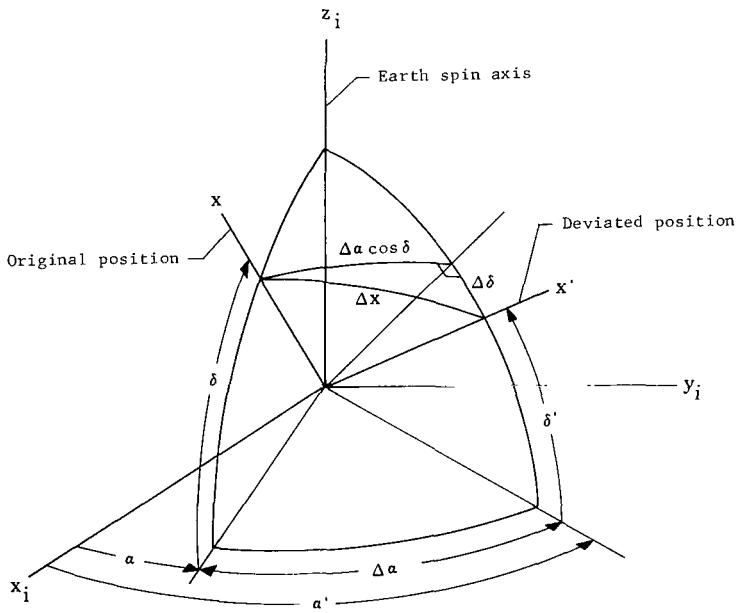

Figure 6.- Total pointing-direction deviation.

equations (4) and either the law of cosines formula

$$\cos \Delta x = \sin \delta \sin \delta' + \cos \delta \cos \delta' \cos (\alpha - \alpha') \tag{15a}$$

or the approximation

$$\Delta x \approx \sqrt{(\Delta\alpha \cos \delta)^2 + (\Delta\delta)^2} \tag{15b}$$

where

$$\Delta\alpha = \alpha - \alpha'$$

$$\Delta\delta = \delta - \delta'$$

and (α,δ) and (α',δ') refer to the original and deviated positions of the instrument axis, respectively.

Computational Results

Six torque cases requiring seven sets of time histories were used to determine the separate and combined effects of the five torques. The results are presented as plots of the pointing direction and state variable deviations obtained as the differences between appropriate pairs of time histories. Similar data were generated for investigating linear characteristics of the torque perturbations, and sensitivities to torque coefficient variations and system design changes. Discussion of the results is concluded with an evaluation of the effects of the torques on attitude prediction.

Time-history plots.- The changes in the pointing direction and state variables obtained for each of the six torque cases are plotted as figure 7 and the corresponding torques as figure 8. Parts (a) to (f) of each figure present the six sets of results in the following order: combined torques, gravity gradient, magnetic moment, eddy current, solar radiation pressure, and aerodynamic pressure. The total deviations produced by the simultaneous action of all five torques, plotted as figure 7(a), represent the differences between an untorqued solution of equations (8) and one having the five torques included. The remaining parts of figure 7 present similar plots of the individual effects of each torque, and the pointing direction error Δx for all six parts was computed from equations (4) and (15). The three frequencies evident in both figures correspond to those of ϕ, ψ, and u, which had respective periods of about 20, 128, and 5680 seconds for the conditions assumed in tables I to III. Quantities which were zero account for the curves missing from some parts of figures 7 and 8.

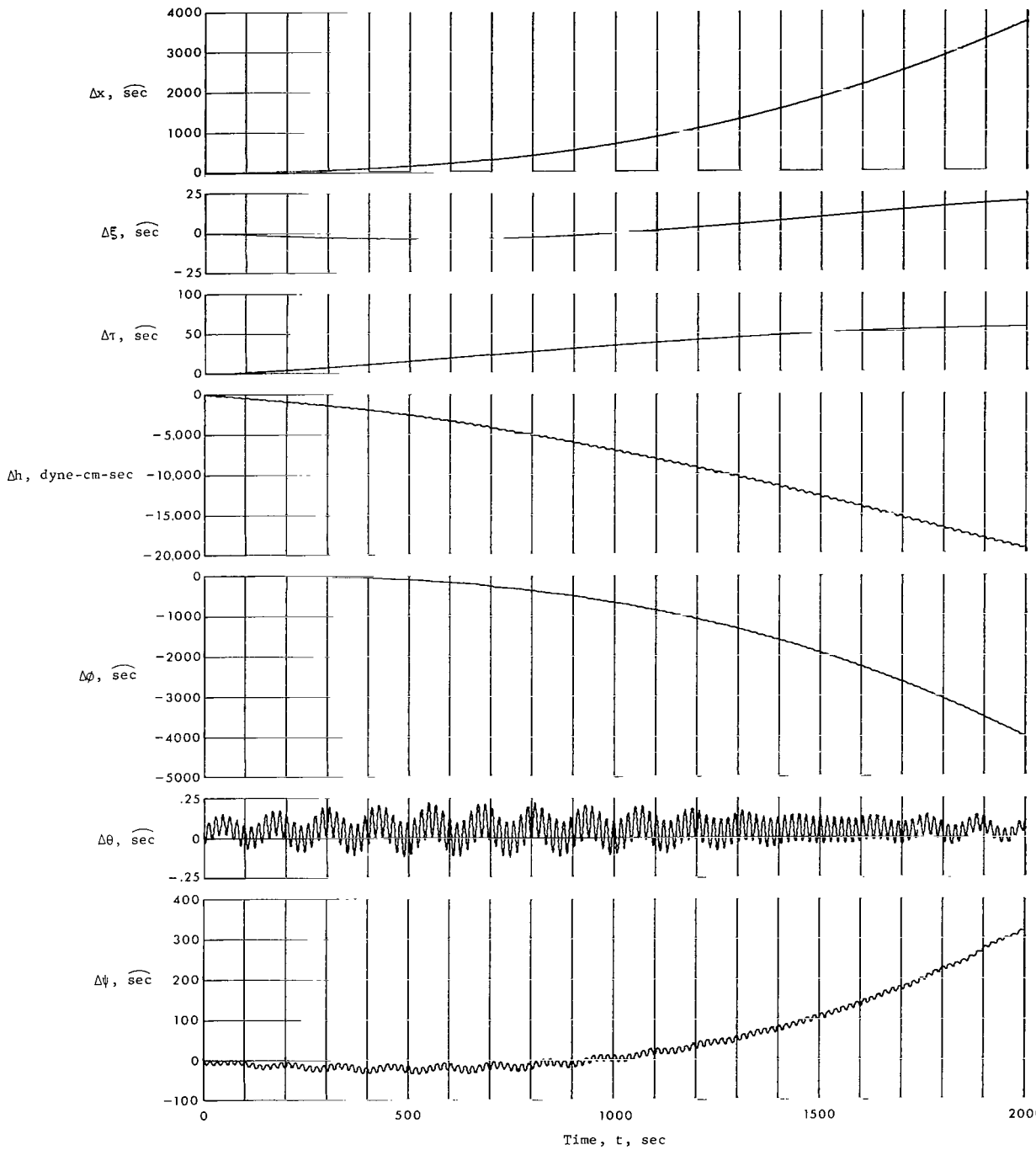

(a) Combined torques.

Figure 7.- Pointing direction and state variable deviations.

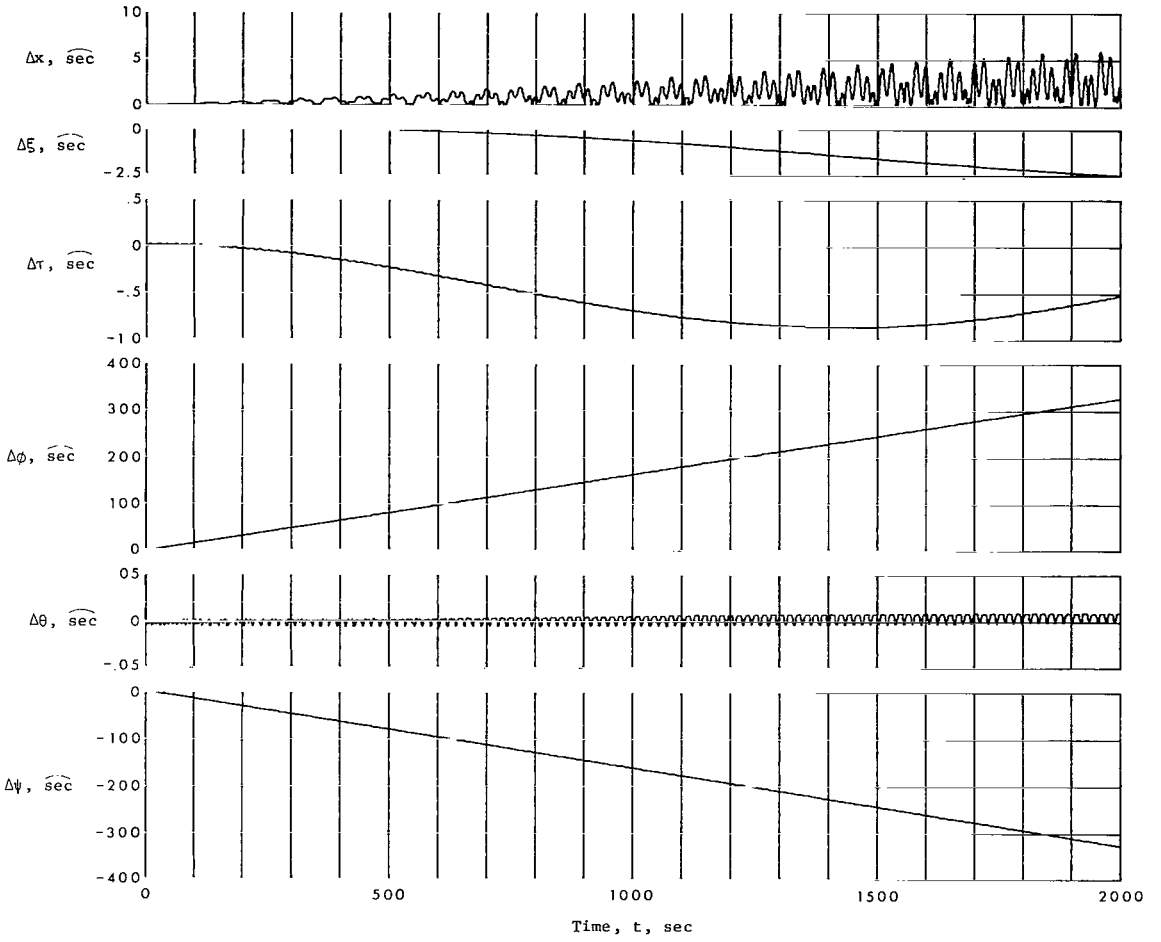

(b) Gravity gradient.

Figure 7.- Continued.

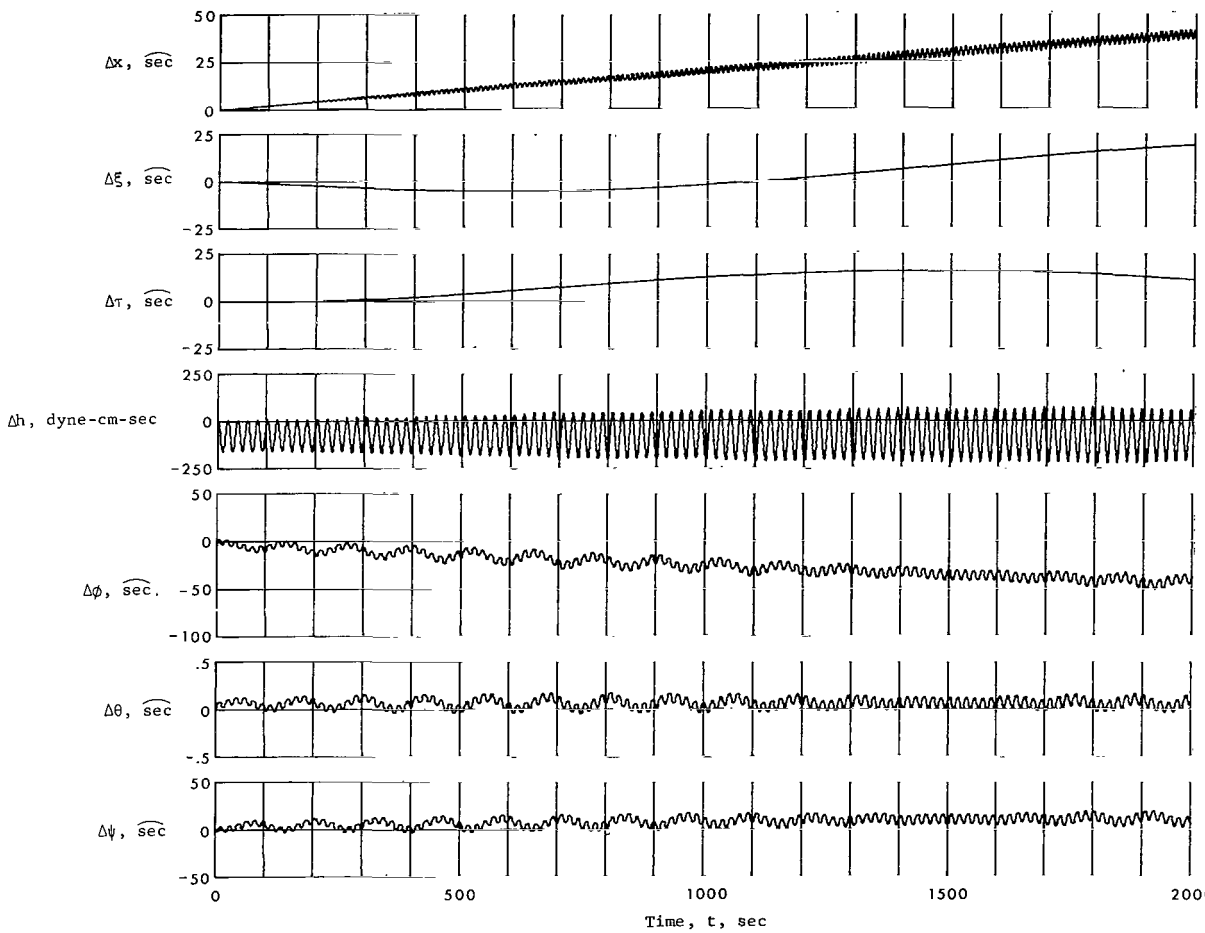

(c) Magnetic moment.

Figure 7.- Continued.

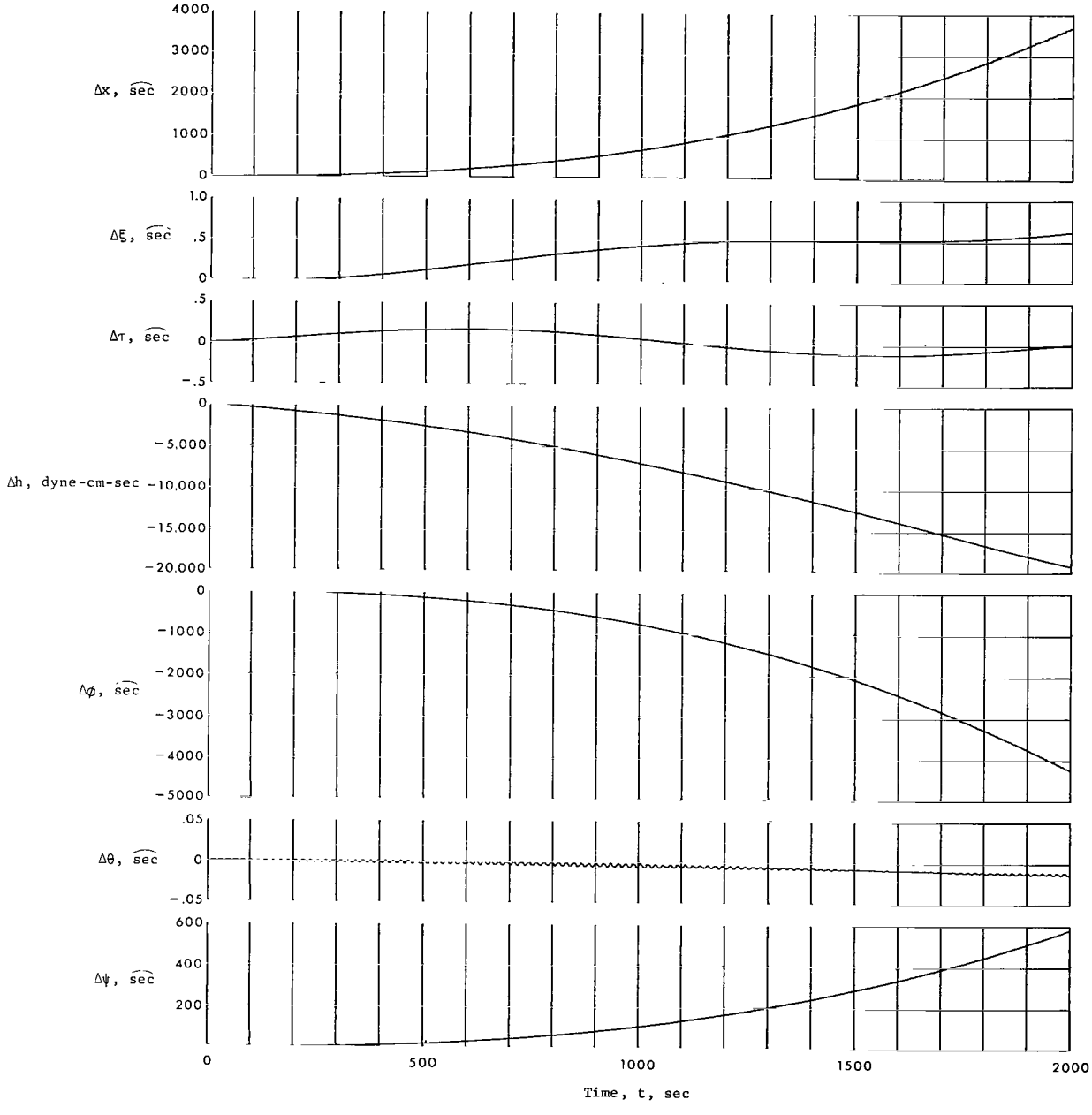

(d) Eddy current.

Figure 7.- Continued.

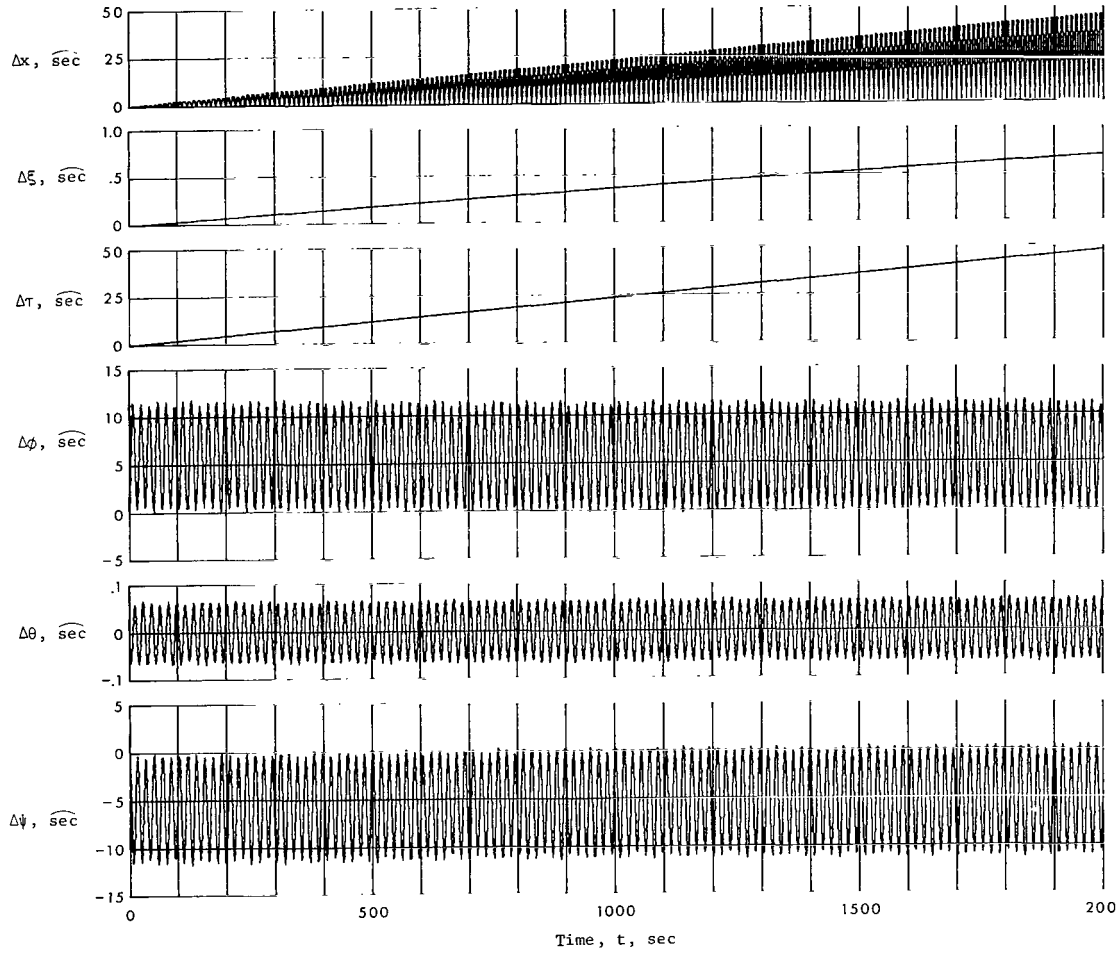

(e) Solar radiation pressure.

Figure 7.- Continued.

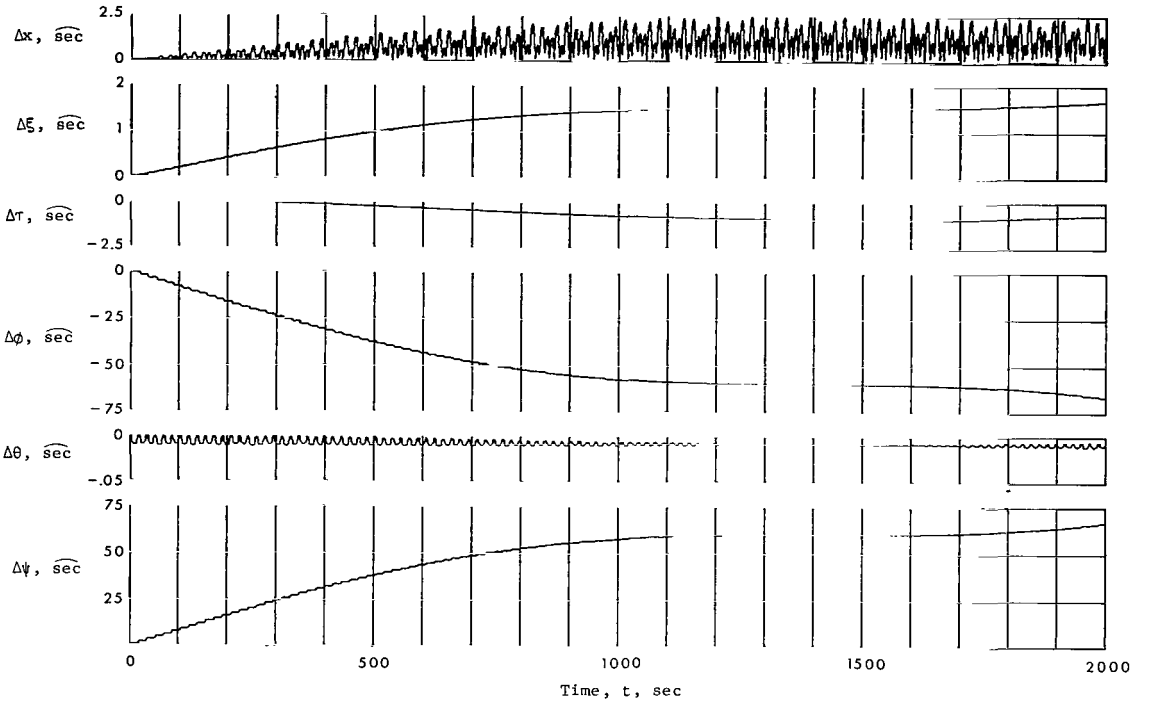

(f) Aerodynamic pressure.

Figure 7.- Concluded.

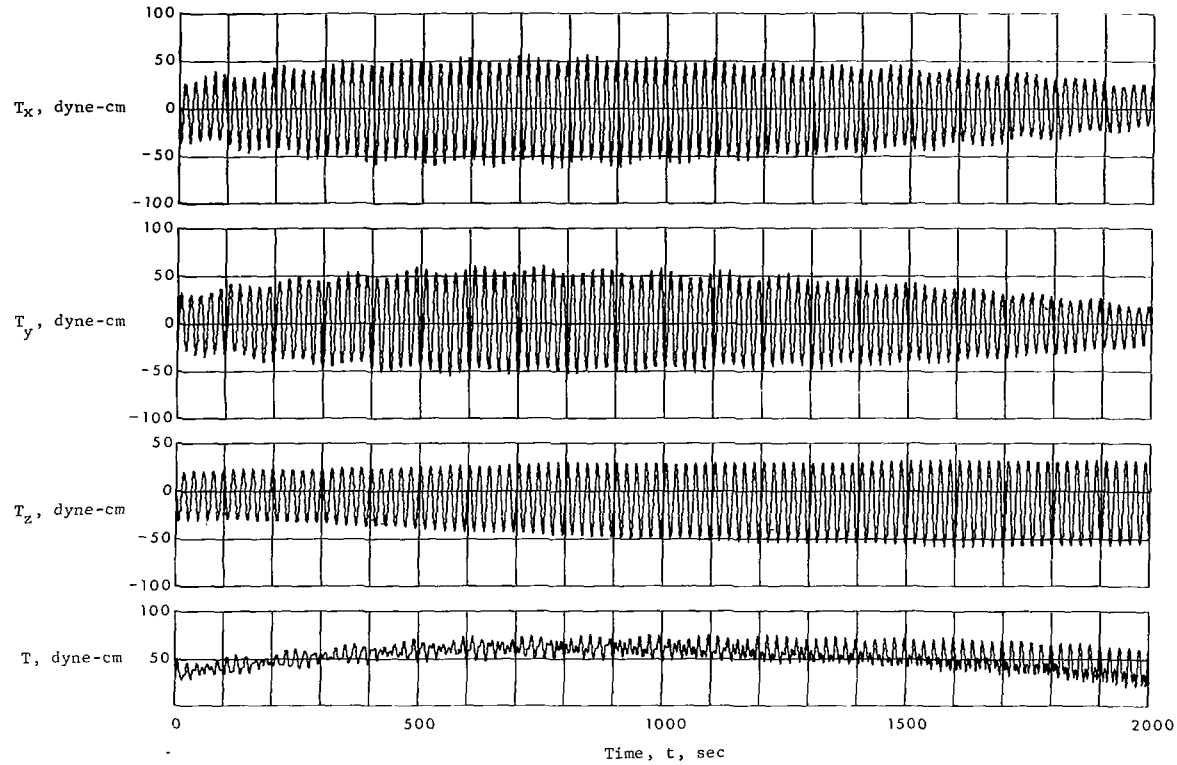

(a) Combined torques.

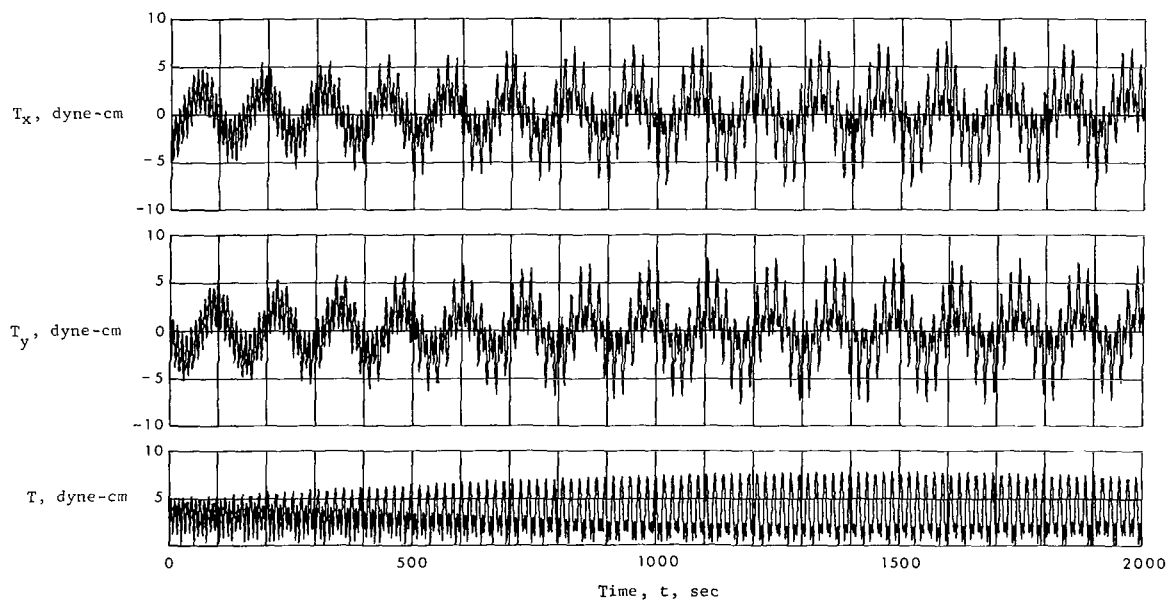

(b) Gravity gradient.

Figure 8.- Environmental torques.

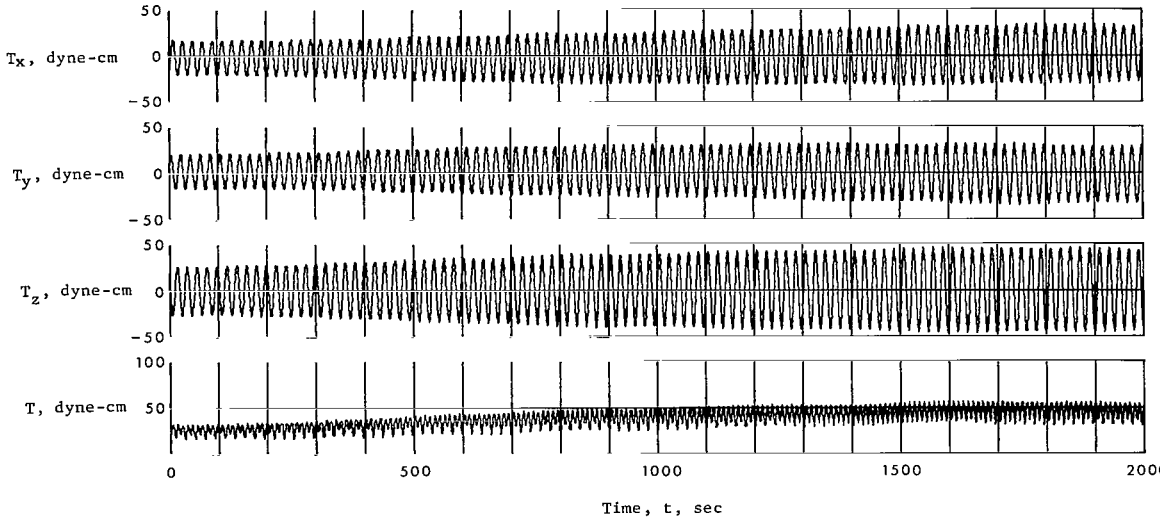

(c) Magnetic moment.

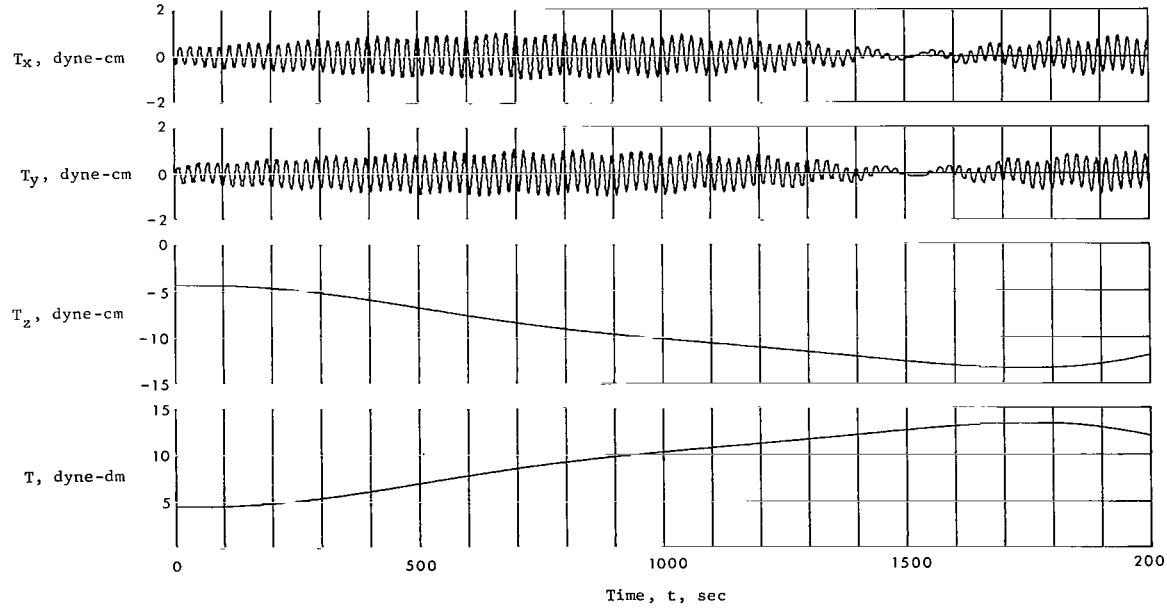

(d) Eddy current.

Figure 8.- Continued.

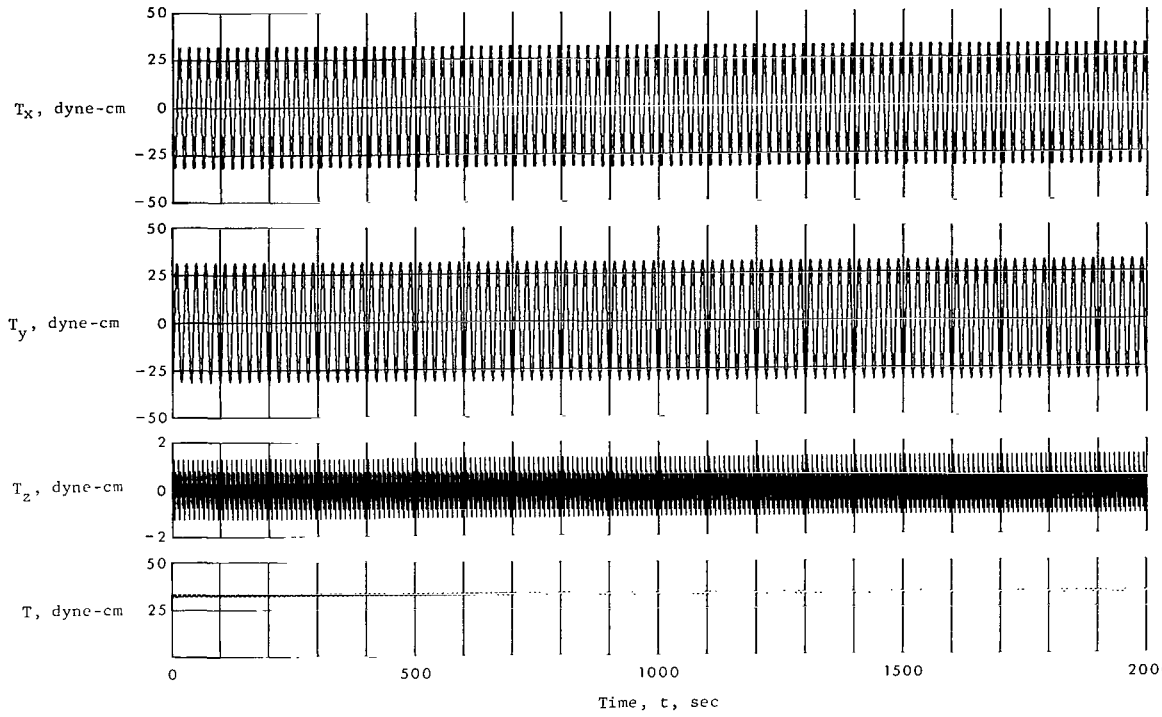

(e) Solar radiation pressure.

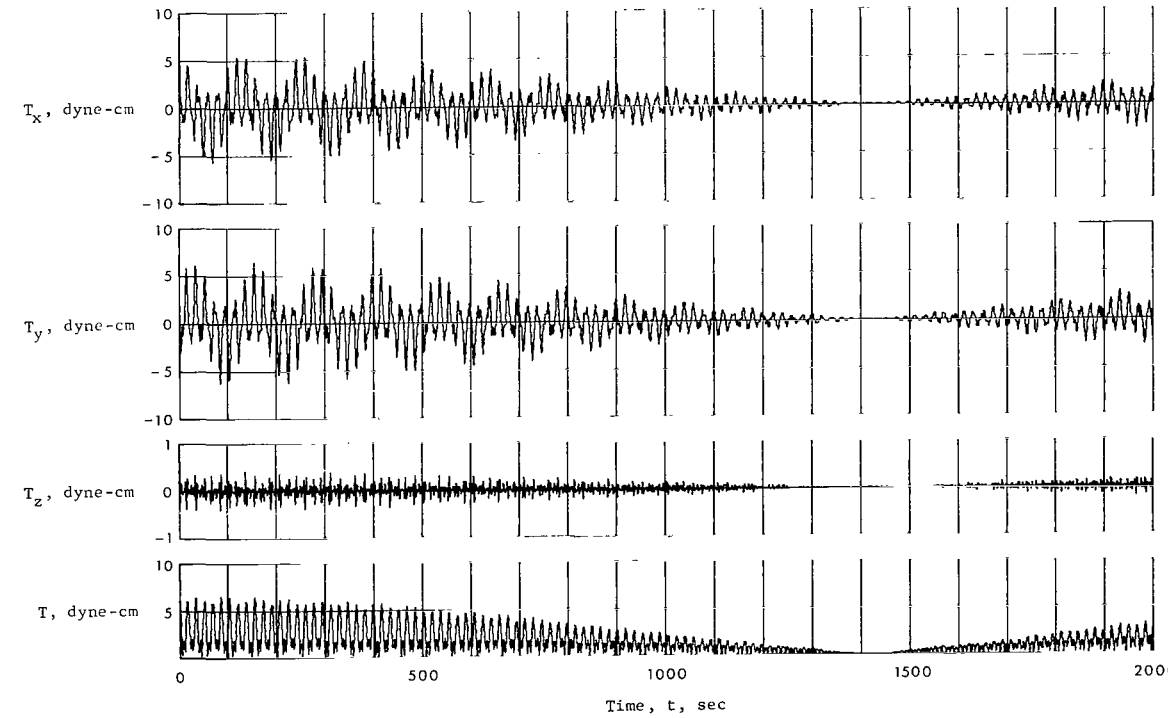

(f) Aerodynamic pressure.

Figure 8.- Concluded.

The results presented as figure 7 indicate that the principal effect of the torques was to despin the spacecraft in nearly an exponential manner with little change in the inertial direction of the principal spin axis. Reference to the plotted curves shows that the instrument-axis pointing direction was progressively altered by roughly 1^{o} over 2000 seconds or about 1/36 000 of its untorqued spin motion. Figure 7 further indicates that Δx was mainly the result of a reduction in spin rate, and was approximately equal to the algebraic sum of $\Delta\phi$ and $\Delta\psi$. This reduction is also evident from the curves for Δh which exhibit a proportional decrease in angular momentum. Because the small coning angle of 0.66^{o} assumed in table III was almost unchanged by the torques (see fig. 7), the principal spin axis remained nearly alined with $\vec{h}$ so that the slight spin axis drift of some 70 arc-seconds is exhibited mainly by the curves for $\Delta\xi$ and $\Delta\tau$. These results show the spin decay to be primarily due to eddy-current torque, and the slight spin axis drift, to solar radiation pressure and magnetic-moment torques. The perturbations caused by environmental torques thus appeared to be very similar to those expected for most rolling-wheel spacecraft.

Linearity.- The linear nature of the torque disturbances mentioned previously, and referred to as an additive property in references 1 and 2, was also evident in the computations being discussed. Addition of the separate perturbations contributed by each torque in the sense of superposition yielded very nearly the same results as those obtained by considering all five simultaneously. The smallness of the torques is clearly the reason linearity is exhibited by the perturbations.

In order to determine the extent or region of linearity, additional solutions to equations (8) were generated with the combined total torques multiplied by factors of 2, 10, 100, and 1000. These factors represent torque levels having respective potentials for angular momentum change ranging from 10^{-7} to 10^{-4} of the nominal magnitude for $\vec{h}$ given in table III. The corresponding amounts by which superposition failed to hold were respectively 0.05, 0.25, and 25 arc-seconds for the first three factors and about 13^{o} for the fourth, thereby indicating fairly good agreement for torque amplitudes up to 100 times their nominal expected levels. The linear region thus defined should also include many other spin-stabilized spacecraft as the torque-to-angular momentum ratio T/h probably will not exceed this 10^{-5} linearity limit in most cases. For example, rough calculations show this ratio to be only 10^{-6} to 10^{-7} for spacecraft such as Tiros, Tiros M, DME-A, and even Telstar and Syncom.

Sensitivity.- The question of sensitivity to possible variations or errors in torque coefficients was easily resolved as linearity also causes the perturbations to be in direct proportion to the torques that produce them. A 10-percent change in the eddy-current coefficient, for example, would be expected to alter the amplitudes of the curves plotted as figure 7(d) by about 10 percent. This property is of interest for estimating the effects

on attitude prediction of variations in some torque coefficients that may occur between the dark and sunlit regions of the spacecraft orbit.

In regard to system design factors, configuration changes in the spacecraft axial-to-transverse inertia ratio and asymmetry were of concern because of their possible effect on the dominant eddy-current torque. For inertia ratios up to 1.5 and asymmetries as large as 10 percent, which includes most rolling-wheel configurations of interest, the torque perturbations exhibited the same linear properties and were very similar to those presented as figure 7. Based on the evaluations performed in reference 1 and appendix B, geometrical factors such as spacecraft panel arrangement should have little effect on the eddy-current and surface-pressure torques unless fairly extensive changes are made or a paddle-wheel configuration is used. Halving and doubling the spin rate also had minor effects on the results, which was as expected since T/h for the eddy-current torque does not change with the magnitude of $\vec{\omega}$ (see eqs. (6), (8), and (12)). As neither the overall nature or linearity of the torque perturbations were altered by moderate system design changes, similar results might be anticipated for other rolling-wheel spacecraft.

Attitude prediction.- As mentioned in the introduction, attitude prediction accuracy was a primary concern in investigating the effects of environmental torques. The prediction error incurred by ignoring a given torque, which can be readily estimated from figure 7 or similar results, was used in references 1 and 2 as a criterion for determining whether any previously modeled torques could be omitted from the computations. This criterion serves to verify which torques must be included but does not account for the effects of possible uncertainties in their coefficients. Assuming the maximum such uncertainty to be 10 percent, reference to figure 7 indicates that only the eddy-current coefficient is likely to cause the specified error bound to be exceeded.

Because the torques were very small, a comparison of their effects on prediction accuracy with those arising from the propagation of state estimation residuals was of interest. The achievable attitude determination accuracy for the horizon measurements spacecraft was estimated to be about 10 arc-seconds, for which equations (8) would be roughly 100 times more sensitive to state variable residuals than to all five torques combined. The resulting attitude error would not be 100 times larger as the effects of some residuals tend to cancel, but still much greater than that incurred by ignoring the torques completely. While state estimation accuracy thus appears to be the more critical problem and places a greater restriction on attitude prediction, the torques are not negligible and should be included.

Comparison of State Variable Systems

The overall results of both studies indicated little reason to favor either choice of state variables for the type of application considered. Although the use of somewhat

different conditions and alternate surface pressure torque models prevented exact comparisons, the two sets of results were essentially in good agreement as mentioned in the introduction. The numerical differences stem mainly from the fact that the computations presented in references 1 and 2 are for worst case conditions, while figures 7 and 8 were generated for nominal ones. The exact comparisons made in conjunction with evaluating Euler-angle singularities further showed that both formulations yield almost identical results under the same conditions. A somewhat more compact analytical format is afforded by the angular velocity formulation, but the angular momentum state variables are simpler functions of time which permit better insight and physical interpretation of the rigid-body motion. With regard to time-averaging the equations of motion as discussed subsequently, the angular momentum variables are much more convenient as the angular velocity equations of motion are awkward and impractical to average.

An additional scheme of interest for evaluating the torque perturbations is the use of time-averaged equations of motion such as those of reference 3. While these equations may cause some loss of accuracy, they simplify the attitude estimation process by greatly reducing the computational burden associated with their numerical integration. The application of this technique to equations (8) to (14) essentially removed the variations due to ϕ and ψ such that the results nearly duplicated figure 7 as viewed with these harmonics deleted. Examination of figure 7 shows that the error introduced by time-averaging also differs for each torque and respectively ranges from about 3 to more than 15 arc-seconds for the eddy-current and magnetic-moment torques. Depending on which torques are included in the computations, time-averaged equations of motion can thus be nearly an order of magnitude less accurate than indicated in references 1 to 3.

CONCLUSIONS

The results obtained from a numerical evaluation and an analysis of the effects of environmental disturbance torques on the attitude of a hexagonal rolling-wheel spacecraft indicate the following conclusions:

1. The torque perturbations are very small and exhibit linearity such that linearized equations of motion yield accurate results over short periods and the separate perturbations contributed by each torque are additive in the sense of superposition.

2. Linearity of the perturbations is not affected by moderate system design changes and should persist for torque-to-angular momentum ratios up to 100 times the nominal expected value, thus indicating that similar behavior might be anticipated for other rolling-wheel spacecraft as many possible applications are included by these conditions.

3. The principal perturbations in most cases will probably be a relatively small spin decay due to eddy-current torque and a slight spin-axis drift caused by solar radiation pressure and magnetic-moment torques.

4. Because of the small torque-to-angular momentum ratio, Euler-angle singularities should not cause computational difficulties or restrict the use of angular momentum state variables.

5. The environmental torques will affect attitude prediction to a much lesser extent than the propagation of attitude estimation residuals in most cases.

Langley Research Center,
National Aeronautics and Space Administration,
Hampton, Va., November 15, 1971.

APPENDIX A

GEOMAGNETIC FIELD COMPUTATIONS

In order to minimize errors in evaluating the magnetic torques, the magnetic field of the earth was computed from the spherical harmonic model and Gaussian coefficients g_n^m and h_n^m of reference 10 which includes terms through 10th order and degree. As the atmosphere is essentially nonmagnetic, the equations for the geocentric field intensity components given in reference 10 may be expressed in terms of the magnetic flux density as

$$\left.\begin{aligned} B_\Theta &= -\sum_{n=1}^{\infty}\sum_{m=0}^{n}\left(\frac{r_a}{r_o}\right)^{n+2}\left(g_n^m \cos m\lambda + h_n^m \sin m\lambda\right)\frac{dP_n^m(\Theta)}{d\Theta} \\ B_\lambda &= \sum_{n=1}^{\infty}\sum_{m=0}^{n}\frac{m}{\sin\Theta}\left(\frac{r_a}{r_o}\right)^{n+2}\left(g_n^m \sin m\lambda - h_n^m \cos m\lambda\right)P_n^m(\Theta) \\ B_r &= \sum_{n=1}^{\infty}\sum_{m=0}^{n}(n+1)\left(\frac{r_a}{r_o}\right)^{n+2}\left(g_n^m \cos m\lambda + h_n^m \sin m\lambda\right)P_n^m(\Theta) \end{aligned}\right\} \quad \text{(A1)}$$

where the Schmidt-normalized associated Legendre functions $P_n^m(\Theta)$ and their derivatives may be evaluated from the recursive formulas

$$\left.\begin{aligned} P_o^o(\Theta) &= 1 \\ \frac{dP_o^o(\Theta)}{d\Theta} &= 0 \end{aligned}\right\} \quad (n = m = 0)$$

$$\left.\begin{aligned} P_n^n(\Theta) &= \sqrt{\frac{2n-1}{2n}}\,P_{n-1}^{n-1}(\Theta)\sin\Theta \\ \frac{dP_n^n(\Theta)}{d\Theta} &= \sqrt{\frac{2n-1}{2n}}\left[\frac{dP_{n-1}^{n-1}(\Theta)}{d\Theta}\sin\Theta + P_{n-1}^{n-1}(\Theta)\cos\Theta\right] \end{aligned}\right\} \quad (n = m \geq 1)$$

$$\left.\begin{aligned} P_n^m(\Theta) &= \frac{2n-1}{\sqrt{n^2-m^2}}\left[P_{n-1}^m(\Theta)\cos\Theta - \frac{\sqrt{(n-1)^2-m^2}}{(2n-1)}P_{n-2}^m(\Theta)\right] \\ \frac{dP_n^m(\Theta)}{d\Theta} &= \frac{2n-1}{\sqrt{n^2-m^2}}\left[\frac{dP_{n-1}^m(\Theta)}{d\Theta}\cos\Theta - P_{n-1}^m(\Theta)\sin\Theta - \frac{\sqrt{(n-1)^2-m^2}}{(2n-1)}\frac{dP_{n-2}^m(\Theta)}{d\Theta}\right] \end{aligned}\right\} \quad (n > m \geq 0) \quad \text{(A2)}$$

which are much more efficient for digital computer programing than the familiar power series expansions for these functions.

As equations (A1) give B_Θ, B_λ, and B_r as functions of r, Θ, and λ, the initial step in computing the desired principal axis components of the geomagnetic field was to express these coordinates in terms of the spacecraft orbital position. The necessary angular relationships for this purpose are illustrated in figure 9, which also indicates the

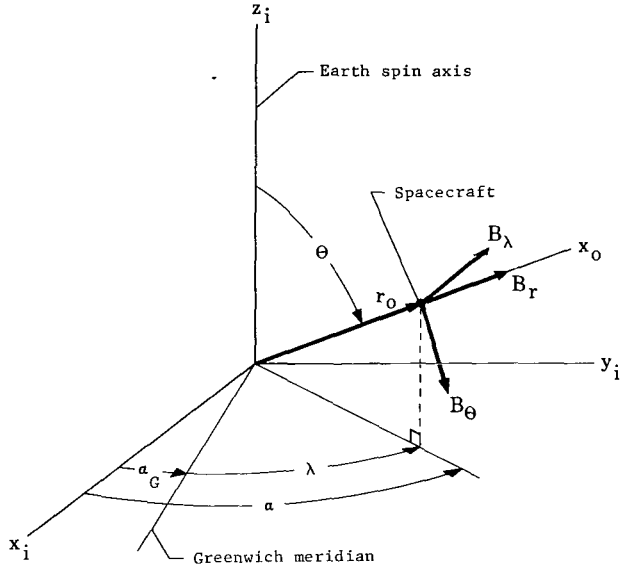

Figure 9.- Geomagnetic field at spacecraft.

spatial directions of B_Θ, B_λ, and B_r. In terms of the notation of figures 2 and 9, expressions for evaluating Θ and λ were obtained by means of the well-known formulas

$$\left.\begin{aligned} \alpha &= \Omega + \tan^{-1}(\cos i \tan u) \\ \Theta &= \cos^{-1}(\sin i \sin u) \end{aligned}\right\} \tag{A3}$$

which appear in standard texts on celestial mechanics. With the geocentric right ascension of the field point at the spacecraft determined from the first of equations (A3), the corresponding east longitude from the Greenwich meridian is

$$\lambda = \alpha - \alpha_G \tag{A4}$$

where

$$\alpha_G = \omega_\oplus t + \alpha_{G_0}$$

and α_{G_o} denotes the right ascension of the Greenwich meridian at a chosen epoch or initial reference time.

After solving equations (A1) to (A4) for the proper values of B_Θ, B_λ, and B_r, the principal axis components B_x, B_y, and B_z may be obtained by means of the transformation

$$\begin{pmatrix} B_x \\ B_y \\ B_z \end{pmatrix} = E(\phi,\theta,\psi)\ H(\xi,\tau)\ G(\alpha,\Theta) \begin{pmatrix} B_r \\ B_\lambda \\ B_\Theta \end{pmatrix} \tag{A5}$$

where $E(\phi,\theta,\psi)$ and $H(\xi,\tau)$ are respectively defined in equations (3) and (2) and

$$G(\alpha,\Theta) = \begin{pmatrix} \sin\Theta\cos\alpha & -\sin\alpha & \cos\Theta\cos\alpha \\ \sin\Theta\sin\alpha & \cos\alpha & \cos\Theta\sin\alpha \\ \cos\Theta & 0 & -\sin\Theta \end{pmatrix}$$

gives the intermediate transformation of B_Θ, B_λ, and B_r to inertial axes.

APPENDIX B

SURFACE-PRESSURE TORQUES

The equations used for calculating the two surface-pressure torques considered in the study were based on the solar radiation and aerodynamic pressure force models of references 8 and 9, respectively. These models express each force in terms of normal and tangential components and were chosen for convenience in obtaining general equations for any surface-pressure torque. The resulting expressions were applied to each of the two torques, then evaluated for the hexagonal spacecraft configuration. Because the resultant forces on the spacecraft panels act at the centers of pressure of the exposed surface areas, a partly computerized semigraphical procedure for locating the corresponding centroids was employed. This approach avoided time-consuming repetitive evaluations of surface integrals by taking advantage of the regular geometry of the panels and overall uniformity of the spacecraft rotational motion and led to efficient approximate expressions for these torques.

General Formulation

With reference to figure 10 let A be that area of a spacecraft panel exposed to a surface pressure. The resultant force $\vec{F}$ then acts through the center of pressure or

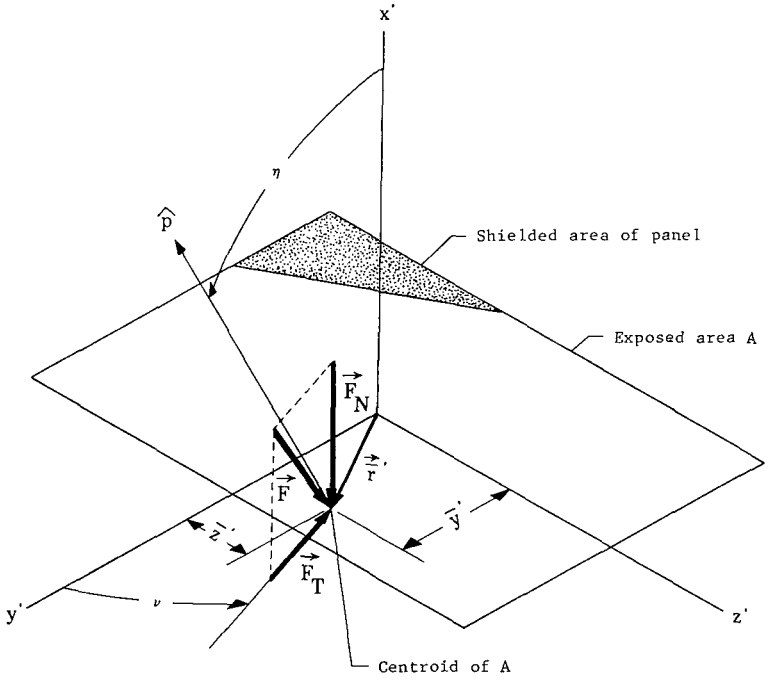

Figure 10.- Surface-pressure force acting on spacecraft panel.

centroid of A as indicated. Relative to the center of the panel, which is the origin of the x'-, y'-, and z'-axes oriented such that y' and z' lie in the plane of the panel with x' normal to it, the centroid of A is located by the vector

$$\vec{\bar{r}}' = \begin{pmatrix} 0 \\ \bar{y}' \\ \bar{z}' \end{pmatrix}$$

where $\bar{x}'$ is zero in all cases. The incident direction of the surface pressure is coplanar with $\vec{F}$ and the x'-axis as indicated in figure 10 and is given by the unit vector $\hat{p}$ the direction cosines of which are

$$\hat{p} = \begin{pmatrix} \cos \eta \\ \sin \eta \cos \nu \\ \sin \eta \sin \nu \end{pmatrix} \tag{B1}$$

The resolution of $\vec{F}$ into components parallel to the x'-, y'-, and z'-axes is

$$\vec{F} = \begin{pmatrix} F_{x'} \\ F_{y'} \\ F_{z'} \end{pmatrix} \tag{B2}$$

where

$$F_{x'} = -F_N$$

$$F_{y'} = -F_T \cos \nu$$

$$F_{z'} = -F_T \sin \nu$$

in which F_N and F_T are, respectively, the normal and tangential components of $\vec{F}$.

The orientation of the panel relative to the spacecraft center of mass is defined by the distance

$$\vec{r} = \begin{pmatrix} x \\ y \\ z \end{pmatrix}$$

between the origins of x', y', and z' and the principal axes x, y, and z, and the angles λ_O, Φ_O, and ζ_O as indicated in figure 11. The angular orientation of the panel

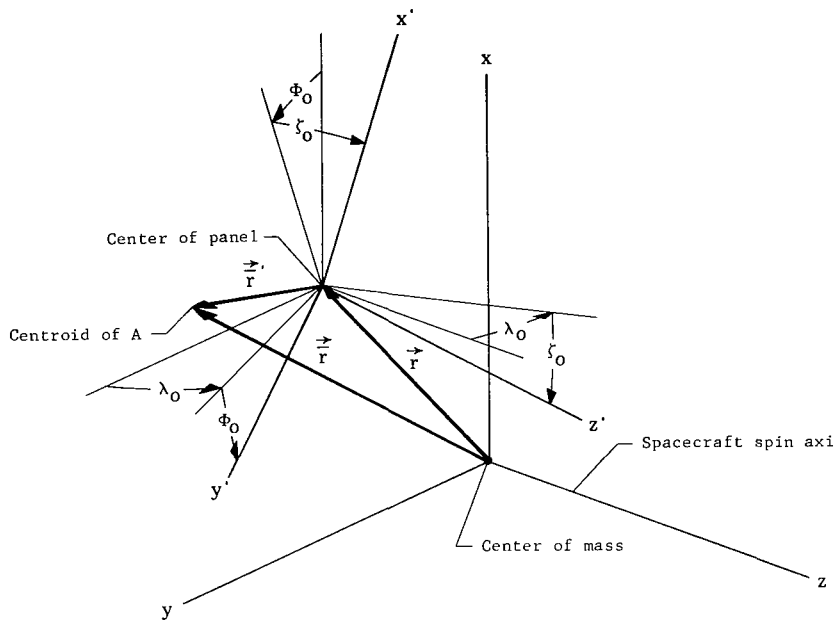

Figure 11.- Orientation of a panel relative to spacecraft center of mass.

with respect to the spacecraft principal axes is given by

$$\begin{pmatrix} x' \\ y' \\ z' \end{pmatrix} = C(\lambda_O, \Phi_O, \zeta_O) \begin{pmatrix} x \\ y \\ z \end{pmatrix} \tag{B3}$$

where

$$C(\lambda_O, \Phi_O, \zeta_O) = \begin{pmatrix} \cos\zeta_O \cos\Phi_O & -\sin\zeta_O \sin\lambda_O + \cos\zeta_O \sin\Phi_O \cos\lambda_O & \sin\zeta_O \cos\lambda_O + \cos\zeta_O \sin\Phi_O \sin\lambda_O \\ -\sin\Phi_O & \cos\Phi_O \cos\lambda_O & \cos\Phi_O \sin\lambda_O \\ -\sin\zeta_O \cos\Phi_O & -\cos\zeta_O \sin\lambda_O - \sin\zeta_O \sin\Phi_O \cos\lambda_O & \cos\zeta_O \cos\lambda_O - \sin\zeta_O \sin\Phi_O \sin\lambda_O \end{pmatrix}$$

The torque exerted on the spacecraft by $\vec{F}$ is

$$\vec{T} = \vec{r} \times \vec{F} \tag{B4}$$

where

$$\vec{\bar{r}} = \begin{pmatrix} \bar{x} \\ \bar{y} \\ \bar{z} \end{pmatrix} = \vec{r} + \vec{\bar{r}}' = \begin{pmatrix} x \\ y \\ z \end{pmatrix} + C\left(\lambda_o, \Phi_o, \zeta_o\right)^{-1} \begin{pmatrix} 0 \\ \bar{y}' \\ \bar{z}' \end{pmatrix}$$

and

$$\vec{\bar{F}} = \begin{pmatrix} F_x \\ F_y \\ F_z \end{pmatrix} = C\left(\lambda_o, \Phi_o, \zeta_o\right)^{-1} \begin{pmatrix} F_{x'} \\ F_{y'} \\ F_{z'} \end{pmatrix}$$

by application of equations (B3) and previous definitions. By using these results, the expansion of equation (B4)

$$T_x = \bar{y}F_z - \bar{z}F_y$$

$$T_y = -\bar{x}F_z + \bar{z}F_x$$

$$T_z = \bar{x}F_y - \bar{y}F_x$$

yields

$$\left.\begin{aligned}
T_x = &-F_N\Big[y\left(\sin\zeta_o\cos\lambda_o + \sin\Phi_o\cos\zeta_o\sin\lambda_o\right) \\
&+ z\left(\sin\zeta_o\sin\lambda_o - \sin\Phi_o\cos\zeta_o\cos\lambda_o\right) + \bar{y}'\cos\Phi_o\sin\zeta_o - \bar{z}'\sin\Phi_o\Big] \\
&- F_T\Big[\left(y\sin\lambda_o - z\cos\lambda_o\right)\left(\cos\nu\cos\Phi_o - \sin\zeta_o\sin\nu\sin\Phi_o\right) \\
&+ \cos\zeta_o\sin\nu\left(y\cos\lambda_o + z\sin\lambda_o\right) - \cos\zeta_o\cos\Phi_o\left(\bar{z}'\cos\nu - \bar{y}'\sin\nu\right)\Big] \\
T_y = &\ F_N\Big[x\left(\sin\zeta_o\cos\lambda_o + \sin\Phi_o\cos\zeta_o\sin\lambda_o\right) \\
&- \bar{y}'\left(\cos\zeta_o\sin\lambda_o + \sin\Phi_o\sin\zeta_o\cos\lambda_o\right) - \cos\Phi_o\left(z\cos\zeta_o + \bar{z}'\cos\lambda_o\right)\Big] \\
&+ F_T\Big\{x\Big[\cos\nu\cos\Phi_o\sin\lambda_o + \sin\nu\left(\cos\zeta_o\cos\lambda_o - \sin\Phi_o\sin\zeta_o\sin\lambda_o\right)\Big] \\
&+ z\left(\cos\nu\sin\Phi_o + \sin\nu\sin\zeta_o\cos\Phi_o\right) - \left(\sin\zeta_o\sin\lambda_o - \sin\Phi_o\cos\zeta_o\cos\lambda_o\right)\left(\bar{z}'\cos\nu - \bar{y}'\sin\nu\right)\Big\} \\
T_z = &\ F_N\Big[x\left(\sin\zeta_o\sin\lambda_o - \sin\Phi_o\cos\zeta_o\cos\lambda_o\right) \\
&+ \bar{y}'\left(\cos\zeta_o\cos\lambda_o - \sin\Phi_o\sin\zeta_o\sin\lambda_o\right) + \cos\Phi_o\left(y\cos\zeta_o - \bar{z}'\sin\lambda_o\right)\Big] \\
&- F_T\Big\{x\Big[\cos\nu\cos\Phi_o\cos\lambda_o - \sin\nu\left(\cos\zeta_o\sin\lambda_o + \sin\Phi_o\sin\zeta_o\cos\lambda_o\right)\Big] \\
&+ y\left(\cos\nu\sin\Phi_o + \sin\nu\sin\zeta_o\cos\Phi_o\right) - \left(\sin\zeta_o\cos\lambda_o + \sin\Phi_o\cos\zeta_o\sin\lambda_o\right)\left(\bar{z}'\cos\nu - \bar{y}'\sin\nu\right)\Big\}
\end{aligned}\right\} \quad \text{(B5)}$$

after substituting equations (B2) and performing some lengthy reductions. Equations (B5) are the desired general expressions for the torque exerted on the spacecraft by a surface pressure acting on a panel having any orientation.

Application to Hexagonal Spacecraft

As all of the spacecraft panels were regular polygons having edges either parallel or normal to the spin axis z, the orientations of the x'-, y'-, and z'-axes for each panel can be chosen so that the angle λ_o is always zero. Equations (B5) then reduce to

$$\left.\begin{aligned}
T_x &= -F_N\left(y \sin \zeta_o - z \cos \zeta_o \sin \Phi_o + \bar{y}' \sin \zeta_o \cos \Phi_o - \bar{z}' \sin \Phi_o\right) \\
&\quad + F_T\left\{z\left(\cos \Phi_o \cos \nu - \sin \Phi_o \sin \zeta_o \sin \nu\right) - \cos \zeta_o\left[y \sin \nu + \cos \Phi_o \left(\bar{y}' \sin \nu - \bar{z}' \cos \nu\right)\right]\right\} \\
T_y &= F_N\left(x \sin \zeta_o - z \cos \zeta_o \cos \Phi_o - \bar{y}' \sin \zeta_o \sin \Phi_o - \bar{z}' \cos \Phi_o\right) \\
&\quad + F_T\left\{z\left(\sin \Phi_o \cos \nu + \cos \Phi_o \sin \zeta_o \sin \nu\right) + \cos \zeta_o \left[x \sin \nu - \sin \Phi_o \left(\bar{y}' \sin \nu - \bar{z}' \cos \nu\right)\right]\right\} \\
T_z &= -F_N \cos \zeta_o \left(x \sin \Phi_o - y \cos \Phi_o - \bar{y}'\right) - F_T\left[x\left(\cos \Phi_o \cos \nu - \sin \Phi_o \sin \zeta_o \sin \nu\right)\right. \\
&\quad \left. + y\left(\sin \Phi_o \cos \nu + \cos \Phi_o \sin \zeta_o \sin \nu\right) + \sin \zeta_o \left(\bar{y}' \sin \nu - \bar{z}' \cos \nu\right)\right]
\end{aligned}\right\} \quad \text{(B6)}$$

For convenience in evaluating equations (B6), the side and end panels of the spacecraft were treated separately.

Side panels.- As illustrated in figure 1, the panels comprising the sides of the hexagonal cylinder are parallel to the spacecraft spin axis so that the angle ζ_o is zero for all six panels. With the spacecraft center of mass located as shown in figure 1, the origins of the x'-, y'-, and z'-axes for each of the six panels lie in the x-y plane at the constant distance $\frac{1}{2}w\sqrt{3}$ from the spin axis z such that

$$\vec{r} = \begin{pmatrix} x \\ y \\ z \end{pmatrix} = \begin{pmatrix} \frac{1}{2}w\sqrt{3} \cos \Phi_o \\ \frac{1}{2}w\sqrt{3} \sin \Phi_o \\ 0 \end{pmatrix}$$

Upon substituting these components of $\vec{r}$, equations (B6) become

$$\left.\begin{aligned}
T_x &= \bar{z}' F_N \sin \Phi_o - F_T\left[\frac{1}{2}w\sqrt{3} \sin \Phi_o \sin \nu + \cos \Phi_o \left(\bar{y}' \sin \nu - \bar{z}' \cos \nu\right)\right] \\
T_y &= -\bar{z}' F_N \cos \Phi_o + F_T\left[\frac{1}{2}w\sqrt{3} \cos \Phi_o \sin \nu - \sin \Phi_o \left(\bar{y}' \sin \nu - \bar{z}' \cos \nu\right)\right] \\
T_z &= \bar{y}' F_N - \frac{1}{2}w\sqrt{3} F_T \cos \nu
\end{aligned}\right\} \quad \text{(B7a)}$$

End panels.- Referring again to figure 1, the ends of the hexagonal cylinder are normal to the spin axis z so that ζ_o as defined in figure 11 is 90^o and 270^o for the solar cell and blank end panels, respectively. In this case the components of $\vec{r}$ are

$$\vec{r} = \begin{pmatrix} 0 \\ 0 \\ \pm\frac{b}{2} \end{pmatrix}$$

and equations (B6) reduce to

$$\left.\begin{aligned} T_x &= F_N\left(\mp\bar{y}' \cos \Phi_o + \bar{z}' \sin \Phi_o\right) + \frac{1}{2} b F_T\left(\pm\cos \nu \cos \Phi_o - \sin \nu \sin \Phi_o\right) \\ T_y &= F_N\left(\mp\bar{y}' \sin \Phi_o - \bar{z}' \cos \Phi_o\right) + \frac{1}{2} b F_T\left(\pm\cos \nu \sin \Phi_o + \sin \nu \cos \Phi_o\right) \\ T_z &= \mp F_T\left(\bar{y}' \sin \nu - \bar{z}' \cos \nu\right) \end{aligned}\right\} \quad \text{(B7b)}$$

where the upper and lower of the double signs apply to the solar cell and blank end panels, respectively.

Solar Radiation Pressure Torque

In terms of the notation employed in figure 10 and equation (B1), the solar radiation pressure force model of reference 8 is

$$\left.\begin{aligned} F_N &= k_1 \cos \eta + k_2 \cos^2 \eta \\ F_T &= k_3 \sin \eta \cos \eta \end{aligned}\right\} \quad \text{(B8)}$$

where

$$k_1 = \frac{2}{3}\rho(1 - s)SA$$

$$k_2 = (1 + s\rho)SA$$

$$k_3 = (1 - s\rho)SA$$

in which S is the intensity of the solar radiation pressure (see table II) and

ρ fraction of incident radiation reflected by A

$1 - \rho$ fraction of incident radiation absorbed by A

s fraction of ρ reflected specularly

$1 - s$ fraction of ρ reflected diffusely

For the hexagonal configuration, the solar cell end panels were assumed to be perfect absorbers of the incident radiation and all remaining panels, perfect specular reflectors. The factors ρ and s are therefore both unity for panels which are perfect reflectors and both zero for those which are perfect absorbers. Hence, for each of the six side panels equations (B7a) reduce to

$$\left.\begin{aligned} T_x &= 2\bar{z}' SA \cos^2\eta \sin\Phi_o \\ T_y &= -2\bar{z}' SA \cos^2\eta \cos\Phi_o \\ T_z &= 2\bar{y}' SA \cos^2\eta \end{aligned}\right\} \quad \text{(B9a)}$$

and for the end panels, equations (B7b) become

$$\left.\begin{aligned} T_x &= \frac{b}{2} SA \sin\eta \cos\eta \cos\nu \\ T_y &= \frac{b}{2} SA \sin\eta \cos\eta \sin\nu \\ T_z &= 0 \end{aligned}\right\} \quad \text{(B9b)}$$

where the resultants of $\bar{y}'$ and $\bar{z}'$ for both ends of the hexagon are zero for the spacecraft orientation corresponding to the conditions listed in table III, and Φ_o for each end become equivalent to arbitrary phase angles which may be set to zero.

The expressions used to evaluate the angles η and ν appearing in equations (B9) were obtained by equating the direction cosines of the unit vector to the sun $\hat{p}$ in the same manner as for equations (4) and (A3). The direction cosines of $\hat{p}$ relative to a spacecraft panel are given by equations (B1) and by

$$\hat{p} = \begin{pmatrix} \cos L \\ \sin L \cos \epsilon \\ \sin L \sin \epsilon \end{pmatrix} \tag{B10}$$

with respect to the geocentric inertial axes x_i, y_i, and z_i defined in figure 2 (also see ref. 11). By using equations (B1) and (B10) and the total transformation given by equations (B3), (3), and (2), the desired relationships are

$$\begin{pmatrix} \cos \eta \\ \sin \eta \cos \nu \\ \sin \eta \sin \nu \end{pmatrix} = C\left(\lambda_O, \Phi_O, \zeta_O\right) E(\phi, \theta, \psi)\, H(\xi, \tau) \begin{pmatrix} \cos L \\ \sin L \cos \epsilon \\ \sin L \sin \epsilon \end{pmatrix} \tag{B11}$$

In order to compute the torques given by equations (B9), the quantities $\bar{y}'$, $\bar{z}'$, A, η, and ν must be determined. As a precise evaluation of this information for even a few spin cycles is not practical because of the large amount of computation required, the feasibility of making approximations was explored. Inspection of equations (B11) shows that the main variations in $\bar{y}'$, $\bar{z}'$, A, η, and ν are due to ϕ and ψ, since the remaining angles are either constant or change very slowly. Hence, an obvious approach was to investigate the variations in the five quantities over a complete cycle of each ϕ and ψ with the rest of the angles in equations (B11) held constant.

Reference to figure 12, which illustrates the nominal initial spacecraft orientation relative to $\hat{p}$ for the assumed 45^o sun-synchronous orbit, indicates the general manner in which the spacecraft panels experience solar radiation pressure. As this orientation will essentially be maintained by attitude control, the blank end panel will always be shielded from radiation pressure such that no torque can arise. The solar cell end will always be fully exposed to the sun, and the side panels will experience partial shielding by the solar cell panels in a periodic manner as the spacecraft spins.

By using a partly computerized semigraphical technique for evaluating the six sets of $\bar{y}'$, $\bar{z}'$, and A for the side panels, the resultant torques given by equations (B9a) and (B9b) were found to be almost unaffected by small variations in $\hat{p}$ caused by the spacecraft coning motion. As the resulting small fluctuations essentially averaged out, for coning angles within the 5^o limit set by attitude control, θ was set to zero with ϕ and ψ replaced by their sum Φ. The error introduced by this approximation amounted to only a few percent for the hexagonal configuration and was judged to be negligible considering the smallness and net effect of the torque itself.

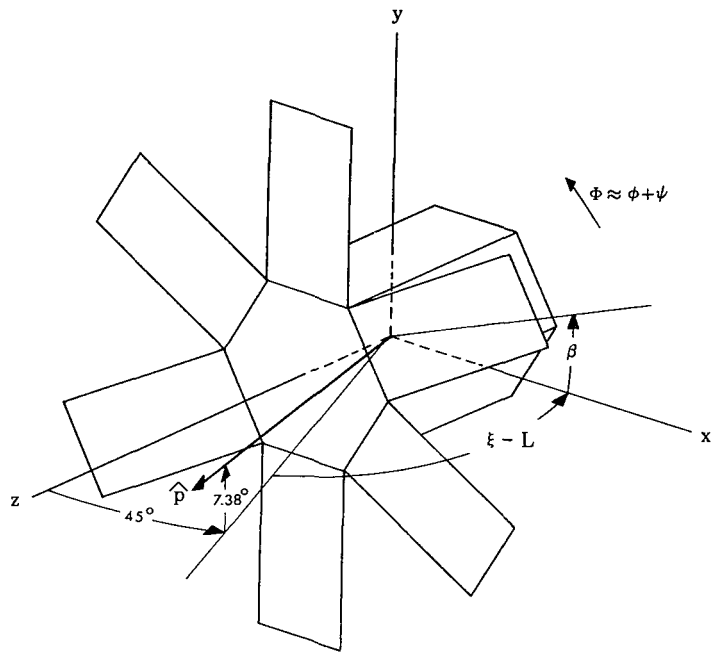

Figure 12.- Nominal spacecraft orientation relative to sun.

With the angles ξ and L nominally constrained to differ by 45^{o} and τ bounded by attitude control limits, the only other effect to consider was the gradual change in the relative elevation of $\hat{p}$ from the initial 7.38^{o} position shown in figure 12. This variation, which annually increases and decreases the elevation of $\hat{p}$ by the obliquity of the ecliptic ϵ, was found to cause a phase shift of the torque components accompanied by minor amplitude changes. The amount of phase shift proved to be equal to the projection of the difference between the angular separations of the spin axis z and $\hat{p}$ from the z_i-axis on to a plane normal to the spin axis z. With this difference denoted by Δp, the resulting phase angle β is given by

$$\tan \beta = \frac{\tan \Delta p}{\cos (\xi - L)} \tag{B12}$$

The value of β for the initial Δp of 7.38^{o} shown in figure 12 was about 10.4^{o}.

Substitution of Φ for the sum of ϕ and ψ, where β is equivalent to sort of a composite Φ_o for the entire panel arrangement, permits reducing equations (B11) to expressions for η and ν which are sinusoids of the angle $\Phi - \beta$. Evaluation of equations (B9) with these simplifications showed the resultant torque components to be mainly functions of $\Phi - \beta$ which appeared to be well approximated as

$$\left.\begin{aligned} T_x &= -R_x \sin(\Phi - \beta) \\ T_y &= -R_y \cos(\Phi - \beta) \\ T_z &= R_z \sin 6(\Phi - \beta) \end{aligned}\right\} \tag{B13}$$

where R_x, R_y, and R_z represent the resultant amplitudes of the SA-factors in equations (B9a) and (B9b). Although $\bar{y}'$, $\bar{z}'$, and A contained the expected harmonic at 6Φ in all three members of equations (B9a), T_x and T_y were dominated by equations (B9b) to the extent that only T_z exhibited a distinct amplitude at 6Φ.

Aerodynamic Pressure Torque

The force model used to evaluate the aerodynamic pressure torque was that of reference 9 and may be expressed as

$$\left.\begin{aligned} F_N &= k_1 \cos^2 \eta \\ F_T &= k_2 \sin \eta \cos \eta \end{aligned}\right\} \tag{B14}$$

where

$$k_1 = 2(2 - \sigma_N) q_o A$$

$$k_2 = \sigma_T q_o A$$

$$q_o = \frac{1}{2} \rho_o v_o^2$$

in which A retains the same meaning defined in figure 10, and the surface reflection coefficients σ_N and σ_T are both usually taken to be 0.8 as explained in reference 9.

By proceeding in the same manner as before, equations (B7a) for the six side panels become

$$\left.\begin{aligned} T_x &= 0.8 q_o A \left\{ 3\bar{z}' \cos^2 \eta \sin \Phi_o - \sin \eta \cos \eta \left[w\sqrt{3} \sin \Phi_o \cos \nu + 2 \cos \Phi_o \left(\bar{y}' \sin \nu - \bar{z}' \cos \nu \right) \right] \right\} \\ T_y &= -0.8 q_o A \left\{ 3\bar{z}' \cos^2 \eta \cos \Phi_o - \sin \eta \cos \eta \left[w\sqrt{3} \cos \Phi_o \sin \nu - 2 \sin \Phi_o \left(\bar{y}' \sin \nu - \bar{z}' \cos \nu \right) \right] \right\} \\ T_z &= 0.8 q_o A \left(3\bar{y}' \cos^2 \eta - w\sqrt{3} \sin \eta \cos \eta \cos \nu \right) \end{aligned}\right\} \tag{B15a}$$

and equations (B7b) for the end panels reduce to

$$\left.\begin{aligned} T_x &= 0.8q_0A\left[3\cos^2\eta\left(\mp\bar{y}'\cos\Phi_0 + \bar{z}'\sin\Phi_0\right) + b\sin\eta\cos\eta\left(\pm\cos\nu\cos\Phi_0 - \sin\nu\sin\Phi_0\right)\right] \\ T_y &= 0.8q_0A\left[3\cos^2\eta\left(\mp\bar{y}'\sin\Phi_0 - \bar{z}'\cos\Phi_0\right) + b\sin\eta\cos\eta\left(\pm\cos\nu\sin\Phi_0 + \sin\nu\cos\Phi_0\right)\right] \\ T_z &= \mp 1.6q_0A\sin\eta\cos\eta\left(\bar{y}'\sin\nu - \bar{z}'\cos\nu\right) \end{aligned}\right\} \quad \text{(B15b)}$$

where the sign convention for equations (B7b) also applies to equations (B15b).

With the direction of the incident aerodynamic pressure $\hat{p}$ assumed to coincide with that of the spacecraft velocity along the orbital path, the direction cosines of $\hat{p}$ relative to the x_0-, y_0-, and z_0-axes defined in figure 2 are

$$\hat{p} = \begin{pmatrix} 0 \\ 1 \\ 0 \end{pmatrix} \quad \text{(B16)}$$

Expressions for evaluating η and ν in equations (B14) were then obtained from equations (B16) and (B1) by using the transformation given by equations (B3), (3), (2), and (1). The resulting relationships are

$$\begin{pmatrix} \cos\eta \\ \sin\eta\cos\nu \\ \sin\eta\sin\nu \end{pmatrix} = C\left(\lambda_0,\Phi_0,\zeta_0\right) E(\phi,\theta,\psi)\ H(\xi,\tau)\ W(\Omega,i,u)^{-1}\begin{pmatrix} 0 \\ 1 \\ 0 \end{pmatrix} \quad \text{(B17)}$$

As with equations (B9), the five quantities $\bar{y}'$, $\bar{z}'$, A, η, and ν must be known to calculate the aerodynamic pressure torques given by equations (B15). The variations in these quantities were evaluated in essentially the same manner as before, and similar approximations were made. However, this task was complicated in two ways by the spacecraft angle of attack. First, because the spacecraft will experience aerodynamic pressure at both positive and negative angles of attack, separate evaluations for each orientation mode were necessary. Secondly, the variation in torque amplitude with angle of attack had to be determined.

Figure 13 depicts the spacecraft orientation relative to $\hat{p}$ for a positive angle of attack. For this case, the side panels will be partially shielded by the solar cell panels in a periodic manner similar to that for solar radiation pressure. The opposite situation occurs for negative values of the angle of attack α_0, as the solar cell panels then experience periodic partial shielding by the side panels.

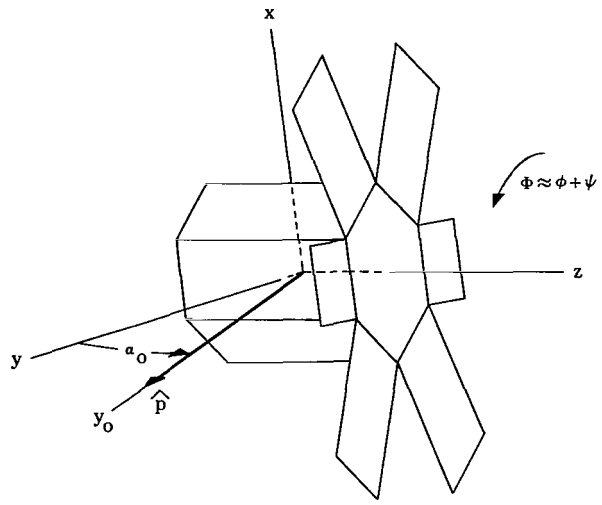

Figure 13.- Spacecraft orientation relative to incident aerodynamic pressure.

In accordance with the assumption in equation (B16) that $\hat{p}$ coincides with y_o of the spacecraft orbit, reference to figure 13 shows that α_o is determined by the scalar product of $\hat{p}$ with a unit vector along the spin axis z. By using the transformation between the x-, y-, and z-axes and x_o-, y_o-, and z_o-axes given by equations (1) to (3) as

$$D = E(\phi,\theta,\psi)\ H(\xi,\tau)\ W(\Omega,i,u)^{-1}$$

to obtain the components of z along the x_o-, y_o-, and z_o-axes the evaluation of this scalar product gives

$$\sin \alpha_o = d_{32} \tag{B18}$$

where d_{32} is the second element in the third row of the D-matrix.

The evaluations for the two orientation modes again showed the variations in $\bar{y}'$, $\bar{z}'$, A, η, and ν to be well approximated with ϕ and ψ replaced by their sum Φ for coning angles up to 5^o. For the case of positive α_o, the contributions from the side panels affected the total torque in much the same way as solar radiation pressure. Because of the particular choice for the panel dimensions, the torques arising from the blank end and side panels exactly canceled each other for negative values of α_o. The net torque was then entirely due to aerodynamic pressure on the back sides of the solar cell panels. The resultant torque components for each mode again were smooth sinusoids of Φ. Because $\hat{p}$ rotates at the orbital frequency, an equivalent elevation change

is produced such that the angle u contributes a phase effect somewhat analogous to β in equations (B13).

The variation in torque amplitude with α_o was determined by evaluating equations (B15) and (B17) over one cycle of Φ for positive and negative values of α_o in 1^o increments covering a range of 5^o. Because of the approximation $\Phi = \phi + \psi$, with the coning angle set to zero, the values for α_o had to be obtained by incrementing τ. This procedure showed the torque amplitudes to be essentially linear functions of α_o over the 5^o range as expected. The resultant torques were surprisingly similar for both orientation modes, except that the z-components were of opposite sign. The respective magnitudes of T_x and T_y for each mode differed by less than 2 percent, while those for T_z were roughly within 5 percent. These results permitted replacing equations (B15) with one set of expressions which apply to both modes.

The resulting approximate equations for T_x, T_y, and T_z were obtained by assuming $\xi = \Omega$, as intended in table III, to permit writing the matrix product $HW^{-1}\hat{p}$ in equation (B17) as

$$H(\xi,\tau)\, W(\Omega,i,u)^{-1}\begin{pmatrix}0\\1\\0\end{pmatrix} = \begin{pmatrix}-\sin u\\ \cos u \cos \alpha_o'\\ \cos u \sin \alpha_o'\end{pmatrix}$$

where $\alpha_o' = i - \tau$ is the effective angle of attack for zero coning angles. Upon substituting this result and approximating $\cos \alpha_o'$ by unity, equations (B15) reduce to

$$\left.\begin{aligned} T_x &= A_x \left|\sin \alpha_o\right| \cos u \cos (\Phi - u)\\ T_y &= -A_y \left|\sin \alpha_o\right| \cos u \sin (\Phi - u)\\ T_z &= -A_z \sin \alpha_o \cos u \sin 6 (\Phi - u)\end{aligned}\right\} \qquad \text{(B19)}$$

where α_o' is now replaced by α_o which will represent the torque more accurately for situations when coning contributes an appreciable part of the effective angle of attack. The absolute value of $\sin \alpha_o$ is necessary for the first two of equations (B19) since the signs of these components do not change with that of α_o as explained previously.

REFERENCES

1. Tidwell, N. W.; Nelson, G. D.; and Lewis, W. J.: Attitude-Referenced Radiometer Study. Vol. I – Attitude Determination System Design. NASA CR-66852, 1969.

2. Tidwell, N. W.: Modeling of Environmental Torques of a Spin-Stabilized Spacecraft in a Near-Earth Orbit. J. Spacecraft & Rockets, vol. 7, no. 12, Dec. 1970, pp. 1425-1433.

3. Foudriat, Edwin C.: Analysis of Limited Memory Estimators and Their Application to Spacecraft Attitude Determination. NASA CR-1654, 1970.

4. Chernous'ko, F. L.: On the Motion of a Satellite About Its Center of Mass Under the Action of Gravitational Moments. J. Appl. Math. & Mech., vol. 27, no. 3, 1963, pp. 708-722.

5. Whittaker, E. T.: A Treatise on the Analytical Dynamics of Particles and Rigid Bodies. Fourth ed., Dover Publ., 1944.

6. Anon.: Spacecraft Gravitational Torques. NASA SP 8024, 1969.

7. Anon.: Spacecraft Magnetic Torques. NASA SP 8018, 1969.

8. Acord, James D.; and Nicklas, John C.: Theoretical and Practical Aspects of Solar Pressure Attitude Control for Interplanetary Spacecraft. Guidance and Control – II, Robert C. Langford and Charles J. Mundo, eds., Academic Press, Inc., 1964, pp. 73-101.

9. Anon.: Orbital Flight Handbook. Vol. 1. NASA SP 33, Pt. 3, 1963.

10. Cain, Joseph C.; Hendricks, Shirley J.; Langel, Robert A.; and Hudson, William V.: A Proposed Model for the International Geomagnetic Reference Field-1965. J. Geomagn. & Geoelec., vol. 19, no. 4, 1967, pp. 335-355.

11. Adams, William M., Jr.; and Hodge, Ward F.: Influence of Solar Radiation Pressure on Orbital Eccentricity of a Gravity-Gradient-Oriented Lenticular Satellite. NASA TN D-2715, 1965.

12. Anon.: U.S. Standard Atmosphere Supplements, 1966. Environ. Sci. Serv. Admin., NASA, and U.S. Air Force.

TABLE I.- SPACECRAFT CONFIGURATION AND TORQUE PARAMETERS

Panel dimensions:	
Height, b, cm	101.60
Width, w, cm	68.58
Length, l, cm	111.76
Moments of inertia and spacecraft weight:	
Transverse, $I_X = I_Y = I$, g-cm^2	2.3885×10^7
Axial, I_Z, g-cm^2	2.6401×10^7
Approximate ratio, I_Z/I	1.2
Approximate launch weight, kg	317.5
Environmental torque coefficients:	
Residual magnetic moments, $M_X = M_Y = M_Z$, A(turn)-m^2	0.07
Eddy current, c, m^4/ohm	1938.8
Solar radiation pressure:	
R_X, dyne-cm	35.532
R_Y, dyne-cm	31.591
R_Z, dyne-cm	0.678
Aerodynamic pressure:	
A_X, dyne-cm	338.87
A_Y, dyne-cm	382.60
A_Z, dyne-cm	24.99

TABLE II.- PHYSICAL PARAMETERS AND GENERAL CONSTANTS

[From ref. 9, except as noted]

Geodetic and geodynamical:	
Equatorial radius, $r_\oplus$, km	6378.2
Mean radius, r_a, km	[a] 6371.2
Universal gravitational constant, μ, km^3/sec^2	398 601.5
Axial rotation rate, $\omega_\oplus$, rad/sec	7.292115×10^{-5}
Obliquity of ecliptic, ϵ, deg	$23^o27'$
Atmospheric and solar:	
Mean atmospheric density at 500 km, ρ_o, kg/m^3	[b] 3.984×10^{-13}
Aerodynamic pressure at 500 km, $q_o = \frac{1}{2}\rho_o v_o^2$, $dynes/cm^2$	[c] 2.4134×10^{-7}
Intensity of solar radiation pressure, S, $dynes/cm^2$	4.5×10^{-5}

[a] Reference 10.

[b] Reference 12.

[c] Calculated using ρ_o and v_o.

TABLE III.- INITIAL SPACECRAFT ORBIT AND STATE VARIABLES

Elements for 500-km 45° sun-synchronous orbit:	
Inclination, i, deg	97.38
Right ascension of ascending node, Ω, deg	45.00
Argument of latitude, u, deg	0.00
Eccentricity, e	0
Altitude, a, km	500.00
Geocentric distance, $r_o = r_\oplus + a$, km	6878.2
Mean motion, $n_o = \sqrt{\mu / r_o^3}$, rad/sec	0.001106798641
Linear velocity along orbital path, v_o, km/sec	7.6164
State variables:	
Angular momentum magnitude, h, dyne-cm-sec	27.9523×10^7
Right ascension of $\vec{h}$, ξ, deg	45.00
Codeclination of $\vec{h}$, τ, deg	97.72
Precession angle, ϕ, deg	0.00
Coning angle, θ, deg	0.66
Proper rotation angle, ψ, deg	0.00
Spin rate, ω_z, rpm	3
Attitude control:	
Maximum angle between orbit normal and spin axis, deg	5

NASA-Langley, 1972 —— 30 L-7359

"The aeronautical and space activities of the United States shall be conducted so as to contribute . . . to the expansion of human knowledge of phenomena in the atmosphere and space. The Administration shall provide for the widest practicable and appropriate dissemination of information concerning its activities and the results thereof."

— NATIONAL AERONAUTICS AND SPACE ACT OF 1958

NASA SCIENTIFIC AND TECHNICAL PUBLICATIONS

TECHNICAL REPORTS: Scientific and technical information considered important, complete, and a lasting contribution to existing knowledge.

TECHNICAL NOTES: Information less broad in scope but nevertheless of importance as a contribution to existing knowledge.

TECHNICAL MEMORANDUMS: Information receiving limited distribution because of preliminary data, security classification, or other reasons.

CONTRACTOR REPORTS: Scientific and technical information generated under a NASA contract or grant and considered an important contribution to existing knowledge.

TECHNICAL TRANSLATIONS: Information published in a foreign language considered to merit NASA distribution in English.

SPECIAL PUBLICATIONS: Information derived from or of value to NASA activities. Publications include conference proceedings, monographs, data compilations, handbooks, sourcebooks, and special bibliographies.

TECHNOLOGY UTILIZATION PUBLICATIONS: Information on technology used by NASA that may be of particular interest in commercial and other non-aerospace applications. Publications include Tech Briefs, Technology Utilization Reports and Technology Surveys.

Details on the availability of these publications may be obtained from:

SCIENTIFIC AND TECHNICAL INFORMATION OFFICE

NATIONAL AERONAUTICS AND SPACE ADMINISTRATION

Washington, D.C. 20546